ERIC M. DESJARDINS

MASTER OF SCIENCE THESIS

THE *IN VIVO* ROLE OF AMP-ACTIVATED PROTEIN KINASE IN THE METABOLIC FUNCTION OF BROWN AND BEIGE ADIPOSE TISSUE

By ERIC M. DESJARDINS, H.B.Sc.

A Thesis Submitted to the School of Graduate Studies in Partial Fulfillment of the

Requirements for the Degree Master of Science

MASTER OF SCIENCE (2016)
Department of Medical Sciences: Nutrition & Metabolism
McMaster University, Hamilton, Ontario, Canada

Title: The *in vivo* role of AMP-activated protein kinase in the metabolic function of brown and beige adipose tissue

Author: Eric M. Desjardins, H.B.Sc.

Supervisor: Dr. Gregory R. Steinberg, Ph.D.

Number of pages: 105

Publications during the acquisition of this degree:

Mottillo EP, **Desjardins EM**, Crane JD, Smith BK, Green AE, Ducommun S, Henriksen T, Rebalka IA, Sakamoto K, Scheele C, Kemp BE, Hawke TG, Granneman JG, and Steinberg GR. Accepted. Lack of Adipocyte AMPK exacerbates insulin resistance and hepatic steatosis through brown and beige adipose tissue function. *Cell Metabolism*.

Smith BK, Ford RJ, **Desjardins EM**, Green AE, Houde VP, Day EA, Crane JD, Mottillo EP, Kemp BE, Tarnopolsky MA, and Steinberg GR. In Revision. Salsalate (salicylate) uncouples mitochondria at subclinical concentrations, improves glucose homeostasis, and reduces liver lipids independent of AMPK β1. *Diabetes.*

Smith BK, Marcinko K, **Desjardins EM,** Lally JS, Ford RJ, Steinberg GR. Submitted. Role of AMP-activated protein kinase (AMPK) for the treatment of non-alcoholic fatty liver disease (NAFLD). *American Journal of Physiology Endocrinology and Metabolism*.

Coleman SK, Rebalka IA, D'Souza DM, Deohare N, **Desjardins EM**, Hawke TJ. Resubmitted. Myostatin inhibition therapy for insulin-deficient type 1 diabetes. *Scientific Reports.*

LAY ABSTRACT

Traditionally, there are two types of adipose tissue that appear and function differently. White adipose tissue (WAT) has evolved to store away energy in an efficient manner for later use. In contrast, brown adipose tissue (BAT) is a unique organ in mammals that has evolved over time to maintain body temperature. In essence, BAT has the ability to burn away calories as heat and is a promising therapeutic target to combat obesity and metabolic diseases such as type 2 diabetes. In our study, we have identified a potential factor that not only promotes BAT activity, but also promotes WAT to function more like BAT. By targeting this factor through drugs, there is potential to increase resting metabolic rate and fight the global epidemic of obesity.

ABSTRACT

Brown (BAT) and white (WAT) adipose tissues are significant contributors to whole-body energy homeostasis. A disturbance in their metabolic function could result in the development of obesity and subsequent metabolic complications. The energy-sensing enzyme of the cell, AMP-activated protein kinase (AMPK), has been vastly studied in skeletal muscle and liver, but its role in BAT and WAT metabolism is elusive. We generated an inducible, adipocyte-specific knockout mouse model for the two AMPK β subunits (iβ1β2AKO) and found that iβ1β2AKO mice were intolerant to cold, and resistant to β3-adrenergic activation of BAT and browning of WAT. These defects in BAT activity were not due to the AMPK-ACC axis, but instead were due to compromised integrity of mitochondria. Mitochondrial morphology, function, and autophagy were all distorted in iβ1β2AKO mice, measured via transmission electron microscopy (TEM), respiration, and immunoblotting, respectively. These findings provide strong evidence that adipocyte AMPK regulates a fine-tuned program that responds to environmental and pharmacological inputs by maintaining mitochondrial integrity through autophagy and subsequent mitochondrial biogenesis in chronic settings.

ACKNOWLEDGEMENTS

The completion of this thesis work would not have been possible without the moral support and guidance of many individuals. To them, I dedicate this work.

I would like to thank Dr. Gregory R. Steinberg for the opportunity to conduct research in his wonderful lab. Your support and trust in me from the very first day has enriched my time here at McMaster University. Your ambition is contagious and I thank you for reminding me that there is always room for improvement.

I would also like to thank my supervisory committee members Dr. Katherine M. Morrison and Dr. Vladimir Ljubicic for their insights on my project. Your kind words go a long way.

I extend my deepest gratitude to Dr. Emilio P. Mottillo, who has been the best mentor I could have possibly asked for. Your passion, knowledge, and understanding of science truly inspire me. Your unmatched dedication, continuous support, patience, and encouragement throughout the last two years will never be forgotten. I wish you and your family nothing but the best in the future.

To all my fellow labmates in the Steinberg lab, past and present, I thank all of you for your assistance, kindness, and most of all, friendship. Adam, Justin, Andrew, Alex, Brennan, Katarina, Emily, Julian, Rebecca, James, Linda, Vivian, Lindsay, Andreas, Vanessa, Rokhsana, Ryan, and Rutu, you all made it fun to come into the lab and work long days.

I would also like to acknowledge Marcia, Aida, Dr. Joaquin Ortega, Irena, and Dr. Thomas J. Hawke for their assistance in the completion of this project.

To Dr. David A. Hood and Dr. Anna Vainshtein, I most certainly would not be where I am today without your positive influences. Your friendship, support, and guidance are greatly appreciated.

Above all, I am truly blessed to have such an incredible family. To my parents, Claude and Sylvie, I am eternally grateful for all that you have sacrificed for me. To my sister, Christine, you have been an exemplar of success and always provide me with an honest opinion. The love from all three of you keeps me going and for this I am extremely grateful.

TABLE OF CONTENTS

LIST OF FIGURES AND TABLES

List of Figures

APPENDIX

List of Tables

CHAPTER II – METHODS AND MATERIALS

LISTS OF ABBREVIATIONS AND SYMBOLS

$\Delta\psi$ – electrochemical proton gradient

AC – adenylyl cyclase

ACC – acetyl-CoA carboxylase

ACC DKI – acetyl CoA carboxylase double knock-in mutations

Adipoq – adiponectin promoter

ADP – adenosine diphosphate

AICAR – 5-amino-4-imidazole carboxamide ribosideAMP – adenosine monophosphate

AMPK – 5' adenosine monophosphate-activated protein kinase

ATGL – adipose triglyceride liapse

ATF2 – activating transcription factor 2

ATP – adenosine triphosphate

β3-AR – beta-3 adrenergic receptor

BAT – brown adipose tissue

BMI – body mass index

BMRGs – browning and mitochondrial related genes

cAMP – cyclic AMP

CAMKK – calcium/calmodulin-dependent protein kinase kinase

CBS – cystathione β-synthase

CL – CL-316,243

CLAMS – Comprehensive Laboratory Animal Monitoring System

CNS – central nervous system

CPT1 – carnitine palmitoyltransferase 1

CPT2 – carnitine palmitoyltransferase 2

CREB – cAMP response-element binding protein

$CreER^{T2}$ – tamoxifen-sensitive Cre recombinase

Cryo-EM – cryomicroscopy

CT – computed tomography

ETC – electron transport chain

FABP – fatty acid binding proteins

FDG – 2-[^{18}F]fluoro-2-deoxy-glucose

FFA – free fatty acids

H^+ – hydrogen ions

HSL – hormone sensitive lipase

iβ1β2AKO – inducible AMPK β1β2 adipocyte-specific knockout

IMM – inner mitochondrial membrane

kDa – kilo Dalton

LC3 – microtubule-associated protein light chain 3

LCFA – long-chain fatty acids

LKB1 – liver kinase B1

mTORC1 – mechanistic target of rapamycin complex 1

MFF – mitochondrial fission factor

NE – norepinephrine

NEFA – non-esterified fatty acids

OMM – outer mitochondrial membrane

p38 – mitogen-activated protein kinase 38

p62/SQSTM1 – sequestosome 1

PBS – phosphate buffered saline

PCR – polymerase chain reaction

PET – positron emission tomography

PGC-1α – peroxisome proliferator-activated receptor gamma coactivator 1-alpha

PKA – cAMP-dependent protein kinase

PP2Cα – protein phosphatase-2Calpha

Raptor – regulatory associated protein of mTOR

RT-qPCR –quantitative reverse transcription polymerase chain reaction

SAT – subcutaneous adipose tissue

SIRT1 – sirtuin 1

SNS – sympathetic nervous system

TCA – tricarboxylic acid

TEM – transmission electron microscopy

Tfam – mitochondrial transcription factor A

TFEB – transcription factor EB

TZDs – thiazolidinediones

UCP1 – uncoupling protein 1

ULK1 – unc-51 like autophagy activating kinase 1

VAT – visceral adipose tissue

VCO_2 – carbon dioxide production

VO_2 – oxygen consumption

WAT – white adipose tissue

WT – wildtype

CHAPTER I - INTRODUCTION

CHAPTER I – INTRODUCTION

1.1 The problem: Overweight and obesity

Overweight and obesity have been labeled as worldwide epidemics and are defined as an abnormal or excessive accumulation of fat that could potentially impair health [1,2]. This accumulation of fat comes from a prolonged exaggeration of caloric intake exceeding caloric expenditure. Due to the rapid rise in obesity prevalence and associated deaths, medical associations across the world have started to formally designate obesity as a disease [3]. In fact, the World Health Organization stated that, in 2014, 39% of adults aged 18 years and above were overweight (BMI 25-30 kg/m^2) and 13% were obese (BMI $\geq$ 30 kg/m^2); which equates to more than 1.9 billion and 600 million people, respectively [2]. The incidence of obesity has more than doubled since 1980, and is projected to surpass a global prevalence of 17 % in men and 21 % in women by 2025, according to the NCD-RisC project [2,4]. More importantly, childhood obesity prevalence is reaching alarming proportions and its prevention and control has become a core priority of the United Nations [5]. Of great concern is that obese individuals are at a higher risk for developing non-communicable diseases such as diabetes, cardiovascular diseases, musculoskeletal disorders, and cancers [2]. Obesity is not only associated with some of the leading causes of disability and death, but is also a large burden on health care systems [6]. For example, in 2008, Wang and colleagues projected that, in the United States, total health-care costs attributable to obesity and overweight would amount to an astounding 860.7-956.9 billion dollars by 2030 [7]. Accordingly, it is of paramount importance to generate new prevention and treatment tactics to combat this multifactorial problem.

1.2 Adipose tissue

Although protuberant adiposity is the most identifiable feature of obesity, research has proven that it is not the amount of fat that dictates whether one's health is at a higher risk, but more so the ability of adipocytes to protect nonadipocytes from a surplus of lipid in times of overnutrition [8]. If this ability is compromised, generalized steatosis can occur and will ultimately lead to lipotoxicity: a state in which organs such as the liver, pancreas, heart, and skeletal muscle can no longer function properly due to a substantial build-up of fatty acids within tissues [9–11]. Adipose tissue is not only regarded as a storage depot for excess energy, but is important in the protection of the body from trauma and for reproduction, amongst other functions. Additionally, in the late 1980's, scientists began identifying serum factors that were released by adipose tissue, now known as adipokines: cytokines secreted by adipose tissue or adipose-derived hormones [12,13] (for review see [14]). Adipose tissue is now regarded as an endocrine organ, as it has the necessary machinery to communicate with other organs and be a key player in energy metabolism, neuroendocrine function, as well as immune function [15].

1.2.1 Adipose tissue types

Traditionally, there are two types of adipose tissue that are morphologically and functionally distinct. White adipose tissue (WAT) has evolved to amass lipids to meet the demand of metabolic tissues during times of starvation [16]. Typically, WAT is composed of white adipocytes containing unilocular lipid droplets and low amounts of mitochondria [17]. There are two major subcategories of WAT, which are defined by general anatomical

locations in rodents and humans: visceral adipose tissue (VAT), which is stored within the abdominal cavity and surrounds internal organs, and subcutaneous adipose tissue (SAT), which is located underneath the skin. Higher accumulation of VAT has been associated with increased morbidity in obesity, while preferential SAT accumulation has been associated with females' increased protection against complications with obesity [18]. It is thought that increased lipid turnover and release of free fatty acids (FFA) via lipolysis from VAT increases the likelihood of developing insulin resistance [19].

In contrast to WAT, brown adipose tissue (BAT) is a unique organ in mammals that has evolved to preserve body temperature homeostasis in cold environments [20]. Brown adipocytes are composed of multilocular lipid droplets, highly developed vasculature with dense sympathetic innervation, and an abundance of iron-containing mitochondria (which give it its "brown-like" colour) containing uncoupling protein 1 (UCP1), which is important for heat production (see Section 1.3) [17]. Thus, BAT has distinct characteristics from WAT that allow it to have a high metabolic capacity to impact whole-body energy metabolism [21,22].

In 1984, Young and colleagues observed that, in response to chronic cold exposure, female BALB/c mice developed a substantial amount of brown fat-like characteristics in the parametrial fat pad; a fat pad that was thought to consist of only white adipocytes [23]. Furthermore, observations were tested biochemically and the group demonstrated that this tissue that had a brown-like appearance morphologically actually contained the heat-producing protein UCP1 (see Section 1.3) [23]. The metabolic plasticity of white adipose tissue, or its ability to recruit UCP1-positive cells that cluster within

WAT depots to elicit a BAT-like phenotype, is a process termed "browning" [17]. These "brite", for brown-in-white, or beige adipocytes have now been shown to be genetically distinct from brown and white [24]. Importantly, these beige adipocytes are believed to have similar molecular characteristics to brown fat deposits in humans [24]. Thus, studying the appearance of these clusters in response to chronic exposures of cold or pharmacological activators, which are notably the same exposures that activate BAT, may prove to be of therapeutic use to increase energy expenditure and improve metabolism in humans.

1.2.2 Discovery of functional brown adipose tissue in humans

A general misconception of the scientific and medical community for most of the 20th century was that BAT was only present and active in humans neonates. However, by assessing 2-[^{18}F]fluoro-2-deoxy-glucose (FDG) uptake using positron emission tomography (PET) and computed tomography (CT), imaging scientists were able to identify a symmetrical tissue in the neck and paravertebral region of the thoracic spine that had a high rate of FDG-uptake and a radiodensity between skeletal muscle and WAT [25,26]. In 2007, Nedergaard and colleagues reported that a substantial fraction of adults, in a limited population from clinical studies with other motives, possessed active BAT that was of metabolic significance [27]. In 2009, the identification of metabolically active BAT in adult humans was further documented [28–31]. Importantly, by obtaining biopsy specimens and assessing morphology and levels of UCP1 mRNA and protein, Virtanen and colleagues identified that this metabolically active tissue was, in fact, BAT [31]. Furthermore, the uptake of ^{18}F-FDG into this area was inversely correlated with BMI, percentage body fat, and fasting plasma glucose levels [28–31]. These reports catalyzed the

renewed interest in BAT research and provided scientists with optimism that activation of this tissue and the browning of WAT could be a useful tool to combat complications associated with overweight and obesity in adult humans.

1.3 UCP1-mediated non-shivering thermogenesis as a therapeutic tool

Producing sixty-times more heat than an equivalent mass of liver, BAT's ability to oxidize a substantial amount of fatty acids has the potential to be a powerful therapeutic target for the treatment of obesity and overweight, as well as type 2 diabetes [32]. It has been well-studied that BAT's ability to consume lipid and produce heat is conferred through a mitochondrial uncoupling process involving the UCP1 [20]. UCP1 was first identified as a 32-kilo Dalton (kDa) protein found only in high abundance in BAT mitochondria and was related to thermogenesis in 1978 by Heaton and colleagues; whereby, a correlation of the protein abundance in BAT mitochondria and the degree of thermogenic adaptation in guinea-pigs was observed [33]. Since then, a multitude of studies have attempted to elucidate the mechanisms by which this protein, and thus the molecular mechanism for heat production, is activated and regulated.

1.3.1 Activation of UCP1

Lipolysis provides the cell with substrate for thermogenesis as well as the ligand for UCP1 activation by liberating FFA. FFA are transported to the mitochondrion by fatty acid binding proteins (A-FABP and H-FABP), transferred into the mitochondrion via the carnitine shuttle system, and are subsequently incorporated into the β-oxidation pathway [34]. The acetyl-CoA yielded from the β-oxidation pathway can then be oxidized in the

tricarboxylic acid (TCA) cycle and provide required substrate for oxidative phosphorylation through the electron transport chain (ETC). As electrons are passed through the ETC complexes, hydrogen ions (H^+) are transferred from the mitochondrial matrix to the intermembrane space, creating an electrochemical proton gradient ($\Delta\psi$). UCP1 dissipates the mitochondrial $\Delta\psi$, through a proton leak across the inner mitochondrial membrane (IMM), uncoupling oxidative phosphorylation [35]. A recent paper suggests that UCP1 acts as a H^+ carrier activated by long-chain fatty acid (LCFA), whereby the LCFA binds to UCP1 on the matrix side of the IMM to initiate H^+ translocation from the intermembrane space to the matrix [36].

1.3.2 Thermogenic program of the adipocyte

It is generally accepted that the thermogenic activation of BAT is regulated by signals from the brain in response to temperature, satiety, and energy reserves [20]. The primary driver of this response involves the stimulation of the sympathetic nervous system (SNS) and subsequent release of norepinephrine (NE) directly onto the brown adipocyte. Concomitant with the dense innervation of BAT is the dense vascularization of BAT [37]. Not only is the vasculature a prerequisite to supply the large amount of substrate and oxygen for the metabolically active tissue, but it is also of crucial importance for the dispersion of heat that is produced [38]. Through β3-adrenergic receptor (β3-AR) activation, a signaling cascade ensues, which involves increases in cAMP via the activation of adenylyl cyclase (AC), and subsequent increases in the activity of the cAMP-dependent protein kinase (PKA).

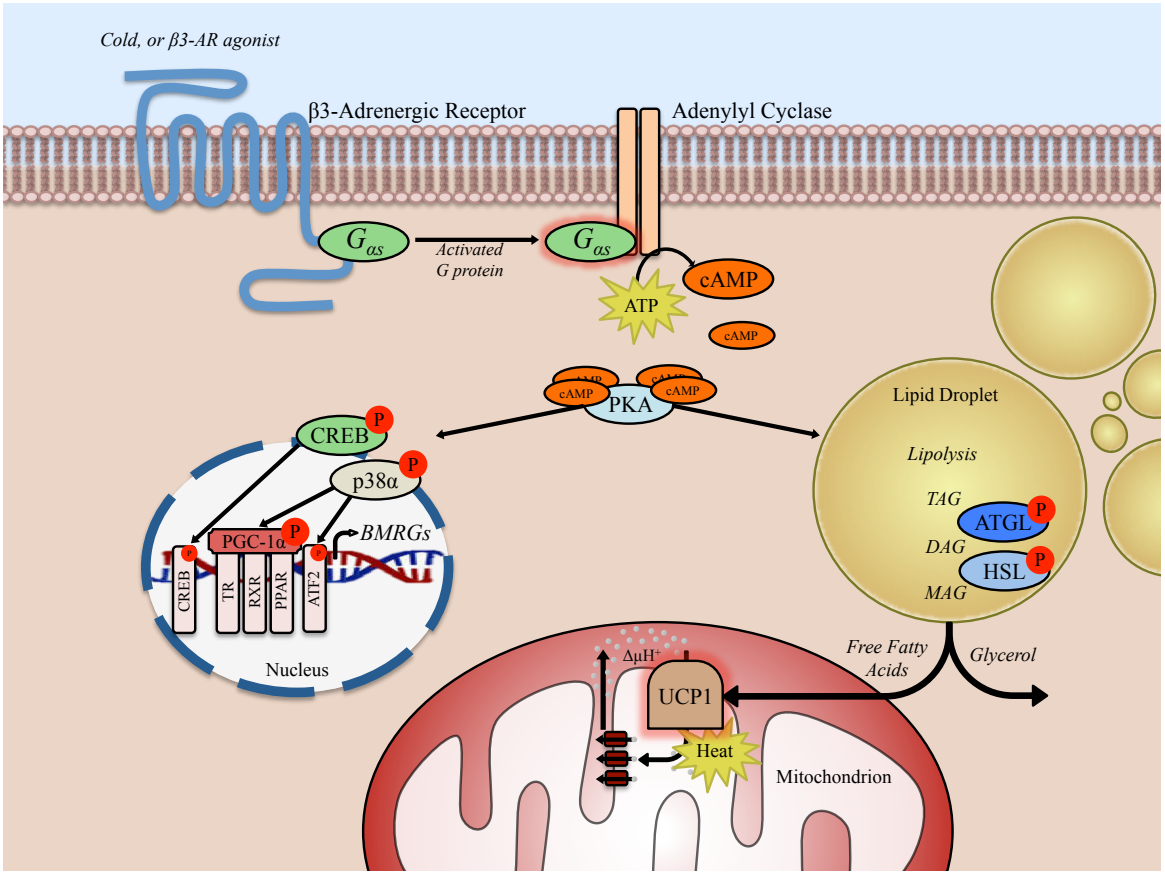

FIGURE 1 – UCP1-MEDIATED THERMOGENESIS THROUGH β3-AR ACTIVATION
Via environmental exposure to cold or the pharmacological activation of the β3-AR, a G_{α}-stimulatory protein increases the production of cAMP from ATP by activating AC. cAMP binds to PKA to increase its activity. Acutely, PKA activates lipolysis enzymes adipose triglyceride liapse (ATGL) and hormone-sensitive lipase (HSL) to liberate FFA for substrate in the β-oxidation pathway and subsequent processes leading to oxidative phosphorylation. FFA activate UCP1 (although the mechanism is still debated). Chronically, PKA phosphorylates proteins CREB and p38α, which are involved in promoting the transcription of browning and mitochondrial related genes (BMRGs), including Ucp1, to increase the cell's capacity to turnover fatty acids as well as uncouple oxidative phosphorylation.

This increases the hydrolysis of triglycerides into FFA and glycerol in lipid droplets (lipolysis) and stimulates the transcription factor cAMP response element-binding protein (CREB) as well as the mitogen-activated protein kinase p38 (p38) [39]. Specifically, p38 has the ability to phosphorylate activating transcription factor 2 (ATF2) and peroxisome proliferator-activated receptor gamma coactivator 1-α (PGC-1α), which induce the transcription of numerous thermogenic genes including *Ucp1* (which have been termed

Browning and Mitochondrial Related Genes; BMRGs) [40]. These are not limited by genes directly involved in responding to adrenergic stimuli and creating heat, but also involve genes that increase general machinery for substrate oxidation. Nevertheless, the mechanisms by which β3-AR activation improves the metabolism of the cell have yet to be fully illuminated and require further investigation.

1.3.3 Energetic control of brown adipocytes

Though the natural activation of BAT is mediated in part by the central nervous system (CNS), more specifically the hypothalamus, the question still remains how the brown adipocyte has the ability to respond to a variety of cues; including energy demand as well as environmental temperature, stress, sex steroids, nutrition, and endocrine factors in a cell autonomous manner [41,42]. To date, the molecular mechanisms by which brown and beige adipocytes balance the use and production of adenosine triphosphate (ATP) are undefined.

1.4 AMPK

5' adenosine monophosphate-activated protein kinase (AMPK) is a highly conserved regulator of energy status in eukaryotic cells, and is activated in response to physiological, hormonal, and nutritional cues that increase the adenosine monophosphate/ adenosine diphosphate to ATP [AMP]/[ADP]: [ATP] ratio (for review see [43]). AMPK has been deemed the energy sensor of the cell, and its activation results in the hindrance of energy-consuming anabolic pathways and the activation of energy-producing catalytic pathways [44]. AMPK is a ubiquitously expressed αβγ heterotrimeric protein comprising of

catalytic alpha (α1, α2), and regulatory beta (β1, β2) and gamma (γ1, γ2, γ3) subunits that can form 12 distinct combinations [45–48]. Different combinations of the isoforms are distributed among distinctive tissue types and play different roles in their respective cells [49]. This redundancy illustrates the importance of the enzyme; providing organisms the ability to immediately respond to changing environments for survival [44].

1.4.1 AMPK regulation by phosphorylation

As the name implies, AMP allosterically activates AMPK and is an important component of the overall activation mechanism [50]. AMP and ADP compete with ATP for two of the four cystathione β-synthase (CBS) domains of the γ-subunit, and upon binding causes conformational changes to AMPK which promote its activation [51]. The major activating phosphorylation site of AMPK is within the activation loop of the α-subunit catalytic domain, on the threonine 172 (T172) residue [52]. When phosphorylated by upstream kinases such as liver kinase B1 (LKB1) and calcium/calmodulin-dependent protein kinase kinase (CAMKK), AMPKα T172 can be autophosphorylated to increase its activity or inactivated by the protein phosphatase-2Cα (PP2Cα) [44,51]. Altogether, the activation of AMPK is a tightly regulated mechanism, substantiating its critical role in the cell.

1.4.2 Role of AMPK as a governor of whole-body energy metabolism

AMPK regulates cellular energy metabolism through direct effects on key metabolic enzymes and gene transcription, and has differential roles in metabolic tissues [44]. For instance, in 2004, Andersson and colleagues found that hypothalamic AMPK

activity was regulated by orexigenic and anorexigenic hormones, ghrelin and leptin respectively, and when activated pharmacologically by 5-amino-4-imidazole carboxamide riboside (AICAR), increased food intake in rats [53]. Conversely, AMPK activation in tissues such as skeletal and cardiac muscle promote an increase in substrate clearance through glucose uptake, glycolysis, and fatty acid oxidation [44]. In the liver, AMPK activation promotes a decrease in lipid-synthesis and increases fatty acid oxidation [43]. This, along with the following topics, provides proof-of-concept that AMPK plays an important role in regulating whole-body energy metabolism.

1.4.3 Current use of AMPK as a therapeutic target

There are a number of pharmacological agents used for the treatment of obesity and type 2 diabetes that are thought to exert their metabolic benefits through the activation of AMPK. For example, metformin, the first-line drug for type 2 diabetes treatment, activates AMPK in the liver to reduce the synthesis of fatty acids and fasting blood glucose, as well as improve glucose tolerance and insulin sensitivity [54]. Additionally, thiazolidinediones (TZDs) acutely activate AMPK in mammalian tissues to exert insulin-sensitizing effects [55]. It has been described that salicylate, a component of acetyl salicylate (Aspirin) that can also be administered as its own dimer salsalate, directly activates AMPK to promote fat utilization and lower plasma fatty acids [56]. Taken together, the effectiveness of these pharmacological agents in diabetic patients proves that targeting AMPK therapeutically has the potential to improve whole-body metabolic parameters.

1.4.4 AMPK regulates fatty acid oxidation

AMPK regulates several arms of cellular metabolism through the phosphorylation of numerous downstream substrates. One of the most well-known functions of AMPK is that it increases fatty acid oxidation through inhibitory phosphorylation of acetyl-CoA carboxylase (ACC) [57]. ACC is involved in catalyzing the carboxylation of acetyl-CoA to malonyl-CoA, which is subsequently involved in the synthesis of fatty acids or in the allosteric inhibition of carnitine palmitoyltransferase 1 (CPT1) [58]. When ACC is phosphorylated, less malonyl-CoA is produced, reducing the allosteric inhibition of CPT1, the rate-limiting step of β-oxidation, and increasing the rate of fatty acid transport into the mitochondrion for subsequent β-oxidation.

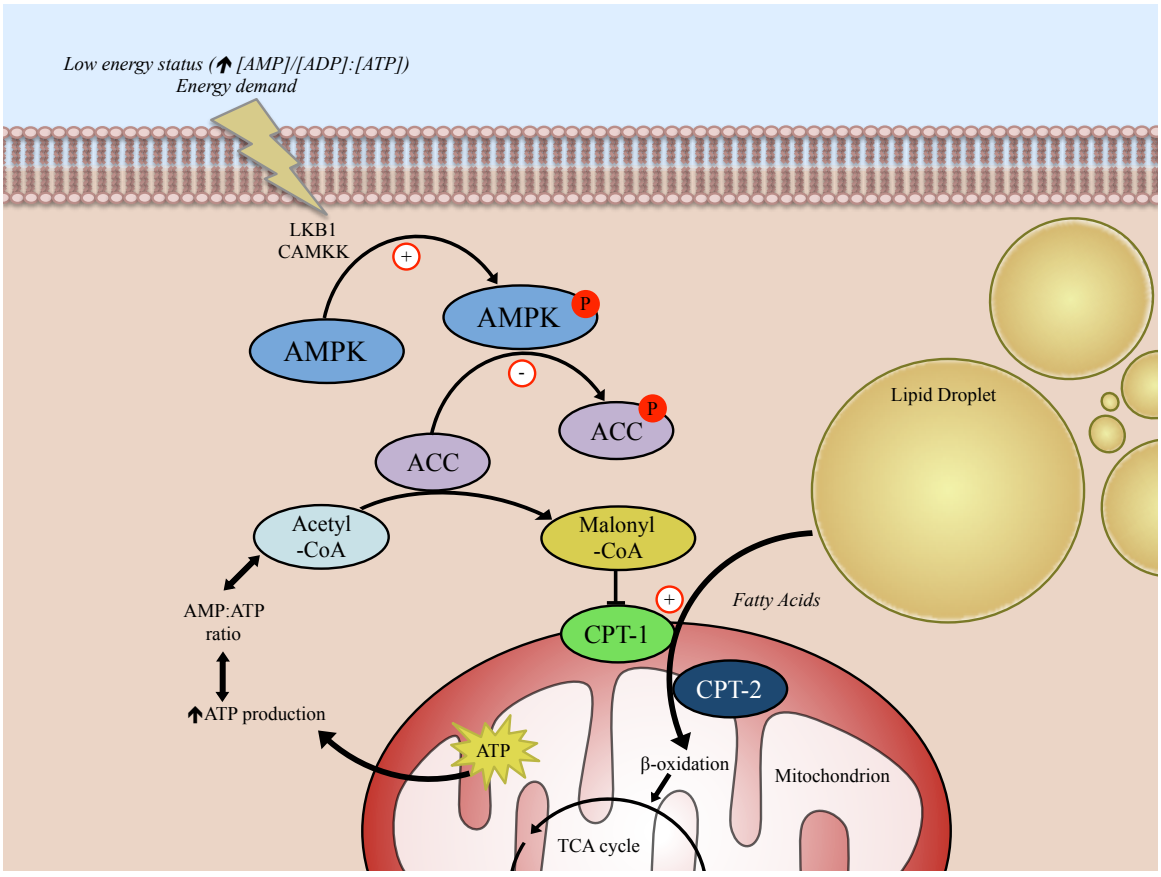

FIGURE 2 –THE INHIBITORY PHOSPHORYLATION OF ACC BY AMPK
In times of energy demand, where [AMP]/[ADP]: [ATP] ratio is increased, AMPK is activated by upstream kinases LKB1 and CAMKK. Phosphorylated AMPKα T172 is able to phosphorylate ACC, and inhibit the carboxylation of acetyl-CoA to malonyl-CoA. Thus, malonyl-CoA can no longer allosterically inhibit CPT1, causing an increase in fatty acid transport from the cytoplasm into the mitochondrion.

1.4.5 AMPK in mitochondrial biogenesis and degradation through mitophagy

Another way AMPK regulates cellular energy metabolism is through improving mitochondrial function and increasing mitochondrial biogenesis. Mitochondria are central components of BAT metabolism, and thus require an intricate balance between biogenesis and degradation. Since its discovery as a cold-inducible coactivator of nuclear receptors linked to adaptive thermogenesis, PGC-1α has become known as the master regulator of mitochondrial biogenesis [59] (for review see [60]). AMPK can mediate an increase in PGC-1α through its direct phosphorylation at T177 and S538, and through indirect effects of deacetylation by sirtuin 1 (SIRT1) [61,62]. Thus, in response to cold or β3-AR agonists, AMPK activity may increase the activity of PGC-1α, which, in turn, increases the transcription of the mitochondrial transcription factor A (Tfam), nuclear-encoded mitochondrial subunits of the ETC, as well as Ucp1 and thermogenic genes [63,64].

In addition to regulating mitochondrial biogenesis specifically through PGC-1α, AMPK has been shown to mediate the degradation of mitochondria through a selective form of macroautophagy (hereafter autophagy) termed mitophagy [65,66]. Mitophagy is a process by which mitochondria are isolated from the mitochondrial network, encapsulated by double-membrane vesicles termed autophagosomes, and are successively transported to the lysosome for proteolytic degradation [66,67]. AMPK can initiate autophagy through the direct phosphorylation of the unc-51 like autophagy activating kinase 1 (ULK1) at

several residues, with S555 being the most studied site, and indirectly through the phosphorylation of regulatory associated protein of mTOR (Raptor) on S792, resulting in the removal of the mechanistic target of rapamycin complex 1 (mTORC1)'s inhibitory action on ULK1 [65,68]. The activation of ULK1 is a key signal for the formation of a mature phagophore, which is needed to capture cytosolic constituents and deliver them to the lysosome [69]. Also involved in this process is the microtubule-associated protein

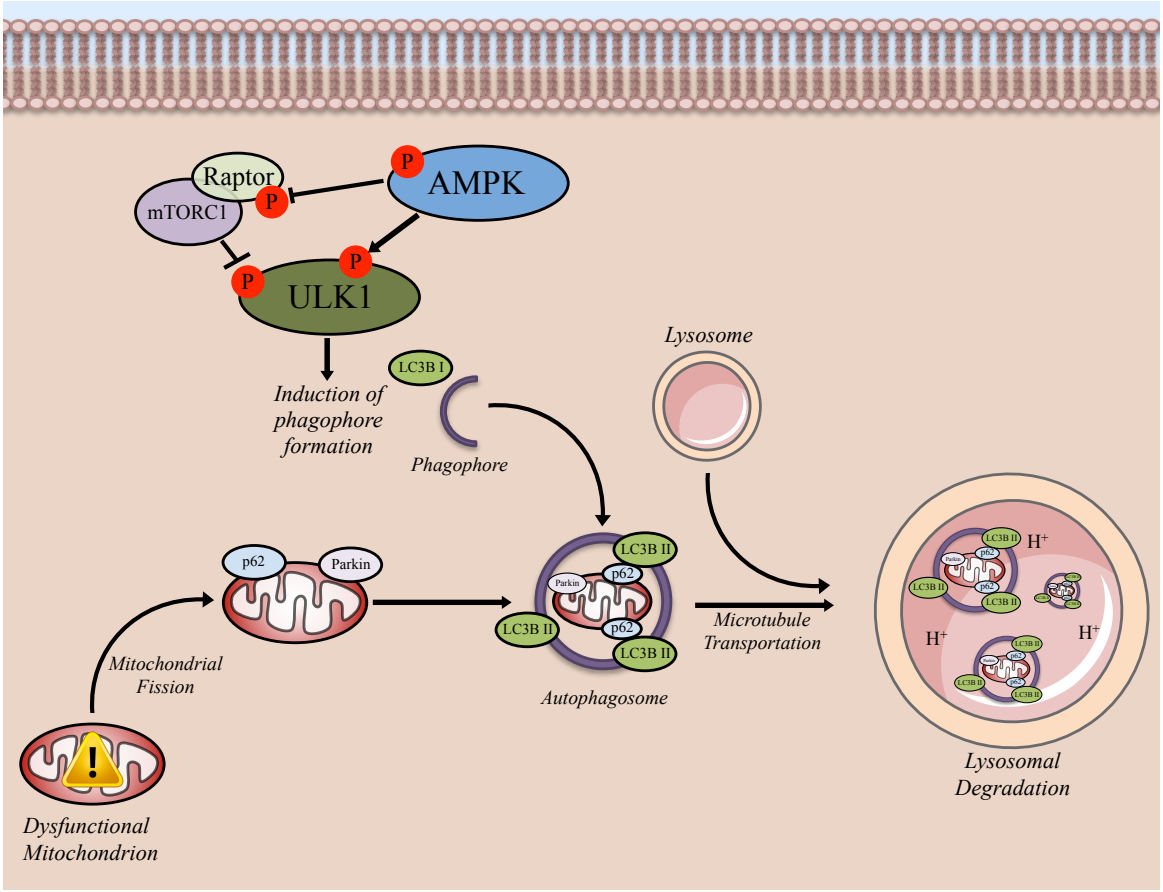

FIGURE 3 –AMPK REGULATES THE INDUCTION OF MITOPHAGY
AMPK can either directly phosphorylate ULK1 or indirectly regulate the activation of ULK1 through its phosphorylation of Raptor and inhibition of the mTORC1 complex. ULK1 is a key signaling enzyme in the induction of phagophore formation, which eventually encapsulates tagged mitochondria for degradation. When mitochondria become dysfunctional, they are tagged by adaptor proteins p62 and Parkin, which interact with polyubiquinated mitochondria and the active form of LC3 (II). Once formed, autophagosomes are transported towards and fused with lysosomes for the degradation and recycling of constituents.

light chain 3 (LC3), which undergoes processing and lipidation in order to become active (LC3 I→LC3 II) [70]. LC3 is responsible for the elongation of the double-membrane vesicle, which transitions from a phagophore to an autophagosome when the membrane has completely encapsulated the constituents [71]. In addition, LC3 II has been found to interact with adaptor proteins that tag polyubiquinated cargo for degradation: p62/sequestosome 1 (SQSTM1) and Parkin, specifically for mitochondria [72,73].

As mentioned previously, AMPK acts as a fuel sensor of the cell, increasing its activation in conditions of energy demand. With a constant need for energy, the cell remodels itself; increasing its machinery for energy production, while ridding itself of inefficient hardware. As such, AMPK can regulate the integrity of the mitochondrial pool: being the fulcrum balancing biogenesis with degradation. What is not known is whether AMPK plays this role in the metabolic plasticity of BAT and WAT.

1.4.6 Stimulation of energy utilization in brown and beige adipose tissue via AMPK

In 2007, Mulligan and colleagues observed that chronic cold exposure stimulated AMPK in the BAT and WAT of mice [74]. It was later shown that AMPK's activation in BAT, along with UCP1 content, was reliant on sympathetic innervation via comparison of denervated and contralateral sham fat lobes in the BAT of mice [75]. However, when these data were tested in the available AMPK-$\alpha1^{-/-}$ mice, there were no distinguishable differences in body temperature between wild-type (WT) and AMPK-$\alpha1^{-/-}$ counterparts [76]. The AMPK-α1-independent effect is perhaps not that surprising, given that AMPK-α2 is expressed in BAT and is upregulated in response to the deletion of AMPK-α1. Thus, the question of AMPK's necessity in the regulation of non-shivering thermogenesis remained

unknown. As AMPK activity is highest in BAT, compared to all other tissues that have been studied, a more thorough examination of this enzyme's role in the stimulation of energy utilization in brown and beige adipose tissues is important [74].

1.5 Objectives and hypotheses

We hypothesized that adipocyte AMPK is required for the induction of non-shivering thermogenesis in BAT and the browning of WAT. In order to test our hypotheses, we have generated a novel, inducible and tissue-specific mouse model for the deletion of AMPK β1β2 in adipocytes (iβ1β2AKO). To determine whether adipocyte AMPK is required for the activation of BAT, we subjected Control and iβ1β2AKO mice to an acute bout of cold, as well as our standardized rodent infrared thermography protocol using the highly selective β3-AR agonist CL-316,243 [77]. Additionally, we tested whether adipocyte AMPK is required for the browning of WAT by subjecting Control and iβ1β2AKO mice to a five-day CL-316,243 challenge; which increases browning of WAT [78]. We sought to define the mechanisms by which AMPK could be mediating effects in brown and beige adipose tissue function, and investigated AMPK's downstream target ACC in this process using mice with Ser-Ala knock-in mutations which block the ability of AMPK to phosphorylate and inhibit ACC. Lastly, we analyzed the role of AMPK in maintaining mitochondrial integrity in BAT by transmission electron microscopy, and assessed autophagic markers via immunobloting and immunohistochemistry.

CHAPTER II – METHODS AND MATERIALS

CHAPTER II – METHODS AND MATERIALS

2.1 Generation of the iβ1β2AKO mouse model

iβ1β2AKO (inducible AMPK β1β2 Adipocyte-Specific Knockout) mice were generated by crossing C57BL/6-backcrossed mice harbouring tamoxifen-sensitive Cre recombinase ($CreER^{T2}$) under the control of the adiponectin promoter B6N.129S-Tg $(Adipoq\text{-}CreER^{T2})^{tm1Jgg}$ with AMPK $\beta1^{flox/flox}$ $\beta2^{flox/flox}$ mice [79,80]. The deletion of AMPK β1β2 was carried out by administering the drug tamoxifen (see below) when mice reached maturity (7-8 weeks of age). All mice, including littermates not expressing $CreER^{T2}$ (Control), received tamoxifen and were subsequently given a minimum of two weeks to recover from the stress. All animal genotypes were determined by PCR using tail endings from an early age and later confirmed via Western Blotting and immunodetection (see below) for $pACC^{S79}$/ACC and $pAMPK\alpha^{T172}$/AMPKα.

2.2 Inducible adipocyte AMPK β1β2 deletion in vivo

Tamoxifen (Cayman Chemicals 13258) was dissolved in 100 % ethanol at 80 °C, then, at 50 °C with gentle vortexing, filtered sunflower oil (Unico) was added to give a final concentration of 20 mg/mL tamoxifen in 10% ethanol sunflower oil [79]. Subsequently, aliquots were made in the cell culture hood and were stored at -20 °C for later use. On days of tamoxifen treatment, aliquots were pre-heated to 37 °C to ensure a complete thaw and a dose of 100 mg/kg was given by oral gavage. Appropriately sized gavage needles were chosen based on the mouse's weight: 22-gage if the mouse was below 20 grams, or 18-gage if the mouse weighed 20 grams or more. All animal facility staff were aware of

tamoxifen-treated mice as there were cards stating "chemical hazard: tamoxifen" along with the days of treatment. Typically, mice were treated with tamoxifen for 5 consecutive days to ensure efficient deletion of adipocyte AMPK.

2.3 Animal experiments

All experiments were approved by the McMaster University Animal Ethics Committee and conducted under the Canadian guidelines for animal research (AUP # 12-12-44). All mice were originally housed in specific pathogen–free microisolator cages in a room kept at 23 °C, and had a 12-hour light/dark cycle with lights on at 0700 hrs. Mice were given a standard chow diet (17 % kcal fat: Diet 8640, Harlan Teklad, Madison, WI) and regular tap water *ad libitum*. All groups were weight matched and randomized to treatment at the beginning of each experiment. The researcher was not blinded to the experimental groups during testing. Animals were excluded from analyses if there were signs of fighting or illness. Female mice were used for cold exposure and β3-AR agonist experiments. Female ACC1-S79A and ACC2-S212A knock-in mutation mice (ACC DKI) were as previously described and used at 3-4 months of age [54]. For cold exposure experiments, mice were maintained at thermoneutrality (29-30 °C) for one week prior to cold challenge to reduce basal sympathetic tone, unless otherwise indicated. Mice had *ad libitum* access to food before the experiment, which was conducted midway through the dark cycle. Food was removed for the short period of time when the animals were placed at 4 °C and no differences were observed in shivering behavior between genotypes. For chronic β3-AR agonist experiments (5D CL), mice were intraperitoneally injected with either 0.5 mg/kg CL or a volume-matched amount of saline for four consecutive days. On

the fifth day, CL-treated mice were given a larger dose of 1 mg/kg. All injections were given around 0900 hrs each day.

2.4 Metabolic measurements

Metabolic parameters were assessed using the Comprehensive Laboratory Animal Monitoring System (CLAMS, Columbus Instruments, Ohio, USA). All monitoring was performed in a room kept between 26 and 28 °C. Animals were housed in separate chambers, with *ad libitum* tap water and milled chow for six to seven consecutive days (with one day for acclimatization). Measurements for oxygen consumption (VO_2), carbon dioxide production (VCO_2), and heat (kcal/hr) were averaged per day, or for the 5D CL challenge up to 6 hours post-injection during the experiment. All other measurements were calculated by summing values for a 24 hr time period, starting at 0700 hrs (Food, Drink), or a Day-Night time period, from 0700 hrs to 1900 hrs being the "Day" (Activity). The monitoring system was not paused for injections; instead, the researcher timed each injection to ensure no time points were missed.

2.5 Non-esterified fatty acids (NEFA) assay

Blood was collected via tail knick (non endpoint) or retro-orbital sinus (endpoint) using heparinized capillary tubes (Fisher Scientific) and placed in eppendorf tubes chilled on ice. Plasmas were isolated by centrifugation set at 0-4 °C and spun at 5000 rpm for 5 minutes. The supernatant was collected, placed in eppendorfs, and stored at -80 °C until further use. NEFAs were measured using the WAKO colourimetric assay. Samples were diluted in 1 x PBS in a 1:5 ratio, for a final volume of 10 μL, and pipetted in duplicates in

a 96-well plate. The standard stock solution of 1mM was serial diluted 6 times to give known concentrations of 500, 250, 125, 62.5, 31.125, and 15.5625 for a standard curve. Once plated, 100 μL of Part A from the kit was added to each well and the plate was placed in the incubator set to 37 °C for 5 minutes. The plate was then read with dual absorbance at 550/600 nm to account for potential haemolysis causing disruption to the colourimetric assay. Following, 50 μL of Part B from the kit was added to each well and was incubated for 5 minutes at 37 °C. A final dual absorbance read was made at 550/600 nm. Appropriate calculations of sample concentrations were used by placing the unit on the standard curve, followed by multiplying the dilution factor to produce units in μM.

2.6 Tissue triglyceride (TG) assay

20-50 mg of tissue was homogenized in chloroform: methanol (2:1) and a portion of the organic phase was dried down, resuspended in isopropanol and assayed for triglycerides using a Triglyceride Colorimetric Assay Kit (Cayman Chemical, MI) [81].

2.7 Thermography

To assess UCP1-mediated thermogenesis, thermography was performed. A treadmill chamber attached to a CLAMS unit was utilized, as well as an adapted version of an infrared thermography protocol that our lab has previously described [77]. Repeated tests of mice were done on two different days, with a minimum of 24 hrs of separation, to allow mice a full recovery from anesthetic. Briefly, each mouse was given an i.p. injection of 0.5 mg/g body weight Avertin (2,2,2-Tribromoethanol dissolved in 2-methyl-2-butanol, Sigma Aldrich) at time 0 and subsequently either given a dose of 0.033 nmol/g

body weight of CL-316,243 (Sigma Aldrich) or an equal volume of 0.9 % sodium chloride at the 2 min time-point. Basal oxygen consumption data was collected for a minimum of 5 mins until the 20 min time-point, as this allows for the oxygen within the treadmill chamber to mix thoroughly, the mouse's VO_2 to stabilize, and the activation of brown adipose tissue with CL to be maximal. Once the 20 min time-point had been reached, the mouse was removed from the treadmill chamber only by its tail (being certain to avoid any contact with the mouse's dorsal side) and placed on a cage top for a thermal image to be taken with the infrared camera (FLiR Systems, T650sc, emissivity of 0.98) at a focal length of 30 cm. Approximately 30 to 50 μL of blood was taken via tail knick for non-esterified fatty acid assay analysis from plasma.

2.8 Histology

Histological samples harvested from mice were initially stored and fixed in 10% formalin, and subsequently processed and stained with haemotoxylin and eosin (H&E) by the Department of Pathology and Molecular Medicine at the McMaster University Children's Hospital. Images were taken using a Nikon 90i Eclipse (Nikon Inc., NY, USA) upright microscope at a magnification of 20X.

2.9 Transmission Electron Microscopy (TEM)

Brown adipose tissue (interscapular) was fixed in 2% glutaraldehyde (2% v/v) in 0.1 M sodium cacodylate buffer (pH 7.4) for at least 24 hours. Thin sections were cut on a Leica UCT ultramicrotome and picked up onto Cu grids. Sections were post-stained with uranyl acetate and lead citrate. The preparation, fixation, and sectioning was performed

by the electron microscopy group at McMaster University Medical Center.

Electron micrographs shown in the two top panels in Figure 8A and additional images necessary for the quantitative analysis in Figure 8B and 8C were obtained in an AMT 4-megapixel CCD camera (Advanced Microscopy Techniques, Woburn, MA) mounted in a JEOL JEM 1200 EX TEMSCAN transmission electron microscope (JEOL, Peabody, MA, USA) operating at an accelerating voltage of 80 kV. Higher magnification electron micrographs for publication in the two bottom panels in Figure 8A were obtained in a FEI Tecnai F20 electron microscope operated at 200 kV. Images were collected in a Gatan K2 Summit direct detector device camera at a nominal magnification 3,500X, which produced images with a calibrated pixel size of 10.35 Å. This detector was used in counting movie mode with ten electrons per pixel per second for 45 seconds exposures and 0.5 seconds per frame. This method produced movies containing 90 frames with an exposure rate of two electrons per square angstrom. Movies were collected using a defocus of 5 μm. Frames were aligned using the program alignframesleastsquares_list.exe and averaged into one single micrograph with the shiftframes_list.exe program from the Rubinstein group (https://sites.google.com/site/rubinsteingroup/home). These programs perform whole frame alignment of the movies using previously published motion correction algorithms [82]. A de-noising filter using Photoshop was applied to the entire images shown in Figure 8A, bottom panels.

To perform the quantification in Figure 8B and 8C, 25 images per sample were acquired by random sampling. Mitochondria with disrupted cristae and total mitochondria were counted from each image, averaged per animal, and then expressed as % cristae

disruption (mitochondria with disrupted cristae over total mitochondria). Criteria for disrupted cristae included any observable disorganization, vacuolization, or dissolution of cristae within mitochondria [83]. The experimenter was blinded when capturing images as well as during the quantification process.

2.10 RNA isolation and real-time quantitative polymerase chain reaction

Chipped tissues were lysed in 1 mL TRIzol reagent (Invitrogen, CA, USA). Samples incubated at room temperature for 5 mins and were centrifuged for 10 mins at 12 000 x g at 4 °C. 200 µL chloroform was added and shaken vigorously before allowing the samples to incubate at room temperature for another 2 mins. The samples were centrifuged again for 10 mins at 12 000 x g at 4 °C before collecting the supernatant. An equal amount of 70 % ethanol was added to the tube containing the supernatant and vortexed. In order to extract and purify RNA, we used the RNeasy kit (Qiagen, CA, USA). Extra precaution was taken and a DNase mixture was used in order to degrade any leftover DNA. A NanoPhotometer (MBI, QC, Canada) was used to dictate the concentration (ng/µL) and purity (260/280, 260/230) of the extracted RNA. RNA was either immediately used or stored at -80 °C. RNA was diluted using RNase-free water to a concentration of 2 µg/13.5 µL, and was then used to synthesize cDNA by DNTPs and random hexamers for 5 mins at 65 °C and cooled to 4 °C, then SuperScript III, First Strand Buffer, and DTT for 5 mins at 25 °C, 60 mins at 50 °C, 15 mins at 70 °C, and cooled to 4 °C (Invitrogen, CA, USA). cDNA was either immediately used or stored at -20°C. Using an optimized mastermix including 1.7 µL RNase-free water, 1 µL 10X Buffer , 1 µL $MgCl_2$ (25 mM), 1 µL dNTPs (2 mM), 0.05 µL Ampli-Taq Gold, and 0.25

µL TaqMan probe per reaction, RT-qPCR was performed with a 10 µL reaction (5 µL diluted cDNA, 5 µL mastermix) in a qPCR thermocycler (Corbett Rotor Gene 6000, MBI, QC, Canada). Within the thermocycler, the samples were incubated at 95 °C for 10 mins to activate the Ampli-Taq Gold, and were amplified with 40 cycles of 10 secs at 95 °C and 45 secs at 60 °C. Slopes were corrected for and thresholds were set at 0.05 using the Corbett Rotorgene software (Corbett Research, Australia). All PCR products and TaqMan probes (see Table 1) were purchased from Invitrogen (CA, USA). Relative gene expression was calculated using the comparative Ct ($2^{-\Delta Ct}$) method, where values were normalized to a housekeeping gene (Ppia), and expressed as relative to control saline.

Table 1 – TaqMan probes purchased from Invitrogen (CA, USA)

Gene	TaqMan Assay ID N°
Cidea	Mm00432554_m1
Cox8b	Mm00432648_m1
Cs	Mm00466043_m1
Hadh	Mm00492535_m1
MT-CO2	Mm03294838_g1
Pdk4	Mm01166879_m1
Ppara	Mm00440939_m1
Ppia	Mm02342430_g1
Ucp1	Mm01244861_m1

2.11 Western blotting and immunodetection

Lysate preparation

Tissues were chipped in approximately 40 mg or 100 mg pieces, for brown adipose tissue and white adipose/liver tissues, respectively. Pieces were placed in cryotubes chilled on ice, containing 300-370 µL of cell lysis buffer (50 mM HEPES pH 7.4, 150 mM NaCl, 100 mM NaF, 10 Na-pyrophosphate, 5 EDTA mM , 250 mM sucrose, 1 mM DTT, and 1 mM Na-orthovanadate, 1% Triton X, and Complete protease inhibitor cocktail (Roche)). Two to three ceramic beads were placed in each cryotube, and a Precellys 24 homogenizer (Bertin Technologies, Paris, France) was set to shake 2 x 20 seconds at 5500 rpm. Samples were then set to rotate end-over-end for 30 minutes at 4 °C. Lysates were then centrifuged at 16 000 x g for ten minutes at 4 °C to separate protein from other remnants. The protein fraction was collected and transferred to a 1.5 mL eppendorf chilled on ice. Lysates were then immediately used or stored at -80 °C.

Sample preparation

To determine the concentration of protein within the lysates, the BCA reagent assay was used. Lysates were diluted 1:20 in ultrapure H_2O (Milli-Q) and standards were provided in the assay kit. Samples were then prepared to a final concentration of 1 µg/µL (unless stated otherwise) using 4x SDS sample buffer (40% glycerol, 240 mM, Tris-HCl pH 6.8, 8 % SDS, 0.04 % bromophenol blue, 5 % β-mercaptoethanol, with a 1:50 dilution of 1M DTT). All samples were boiled at 95 °C for 5 mins before being loaded for Western blotting, with the exception of samples being probed for the MitoProfile total

OXPHOS rodent antibody cocktail (room temperature to avoid the degradation of complexes).

SDS-PAGE, transfer, and blocking

SDS polyacrylamide gels were prepared the day prior to running gel electrophoresis and were stored in dampened paper towels at 4 °C overnight. 7.5, 10, or 12 % gels were made, depending on the size of the protein being blotted for. 20 μg of protein was loaded into each well for ACC, AMPKα, Raptor, ULK1, LC3B, p62, PGC-1α, and AMPK β1β2. For BAT samples, 5 μg of protein was loaded for UCP1 and total OXPHOS. For iWAT samples, 15 μg of protein was loaded for total OXPHOS and 20 μg for UCP1. β-tubulin was used as a loading control for total protein blots. Electrophoresis was run at 90 V through the stacking gel and 120 V through the separating gel at room temperature. Separated proteins were transferred onto nitrocellulose or PVDF membranes electrically at 90 V for 90 mins using wet transfer techniques. Subsequently, membranes were rinsed in 1 x Tris-buffered saline (TBS, 50 mM Tris, 150 mM NaCl, 1 M HCl, pH 7.4) for 5 mins then blocked in 5 % bovine serum albumin (BSA) or 5 % skim milk in 1 x TBS with 0.1 % tween-20 (TBST) for 1 hour at room temperature.

Antibody incubation, immunodetection, and densitometry

Membranes were cut and incubated in primary antibody (see Table 2) with 5 % BSA in TBST at 4 °C on a rocker overnight. On the following day, membranes were washed 3 x 10 mins with TBST and incubated with appropriate secondary antibody (see Table 2) in 5 % BSA in TBST for 1 hour at room temperature. After 4 x 10 mins wash in TBST, proteins of interest were imaged using electrochemiluminescence. All phospho

bands were detected first, then membranes were stripped using Restore (ThermoScientific) for 30 mins at 37 °C and reprobed for total bands overnight. If the protein of interest was close to 50 kDa, it was detected first, then stripped and reprobed, similarly to above, for the loading control β-tubulin. Densitometry was performed using Image J software (National Institutes of Health, Bethesday, USA). All phospho/total proteins were converted to ratios and expressed as relative to control, meanwhile other proteins were normalized to β-tubulin/β-actin and expressed as relative to control.

2.12 Cytochrome *c* oxidase (COX) activity assay

COX activity was measured using homogenates in cell lysis buffer (same as Western blotting lysates). Samples were frozen and thawed three times before their use, to ensure proper membrane disruption. Reduced cytochrome c (2 mg/mL; Sigma-Aldrich C2506) was prepared in 10 mM KPO4 (KH2PO4 Sigma P5655, K2HPO4 Sigma P8281) and 0.08 mg/mL sodium dithionite (Sigma 157953). Once prepared, the solution was kept from light, pre-heated to 30 °C, and used within 30 minutes. Briefly, 4 samples of BAT (10 µL) or iWAT (20 µL) were added in a column of a 96-well plate, in duplicate, and mixed with 250 µL of fully reduced cytochrome *c*. A kinetic reading was set at 550 nm, reading every 10 seconds for a total of 9 times in a Synergy H4 microplate reader (Gen5 software; Biotek, Vermont). The average slope was then normalized to protein content determined by BCA protein assay using the following equation. Values were expressed as relative to control.

$$COX\ Activity\ (nmol/min/mg) = \frac{\frac{Average\ Velocity\ Slope}{18.5}}{\frac{[Protein] \times Sample\ Volume}{1000}}$$

2.13 *Ex vivo* fatty acid oxidation

The *ex vivo* fatty acid oxidation protocol was adapted from previously described [84]. 10-20 mg of dissected BAT or 50-70 mg of WAT was gently minced and placed to incubate for 1 hr at 37 °C shaking at 80 rpm in 2 mL of HEPES-buffered Krebs Ring Buffer (HKRB; Sigma, 10 mM HEPES, pH 7.4) with 1 % bovine serum albumin (BSA), 200 μM palmitate, 200 μM L-carnitine, and 2 μCi [1-^{14}C] palmitate within a crafted CO_2 capture system. A glass vial was used to incubate the tissue in solution while an eppendorf containing 450 μL benzethonium hydroxide was used to capture the CO_2. After an hour of incubation, tissues were removed and 1 mL 1M acetic acid was added to the glass vial, ensuring the cap was immediately shut tight. Tissues were blotted dry and weighed. The solution was incubated for another hour at 37 °C before removing the eppendorf containing the captured CO_2. This tube was placed in a scintillation vial before adding 4 mL of scintillation fluid to shake and bring for counting. Values were expressed as nmol palmitate per gram, calculated by the following equation:

$$\frac{\frac{CO_2\ counts - Blank\ counts}{Specific\ Activity\ (counts/\mu mol)}}{Tissue\ weight\ (g)}$$

All counts were expressed as disintegrations per minute (dpm).

Table 2 – Antibodies used for immunoblotting

Primary Antibody	Company (Product #)	Dilution	Secondary Antibody	Dilution
$pACC^{S79}$	CST (11818)	1:1,000	Rabbit IgG HRP-linked CST (7074)	1:10,000
ACC	CST (3676)			
$pAMPK\alpha^{T172}$	CST (2535)			
AMPKα	CST (5831)			
$pRaptor^{S792}$	CST (2083)			
Raptor	CST (2280)			
AMPK β1β2	CST (4150)			
UCP1	ADI (UCP11-A)			
PGC-1α	Millipore (AB3242)			
$pULK1^{S555}$	CST (5869)			
ULK1	CST (8054)			
LC3B	CST (3868)			
SQSTM1/p62	CST (8025)			
MitoProfile OXPHOS	Abcam (ab110413)	1:5,000	Mouse IgG HRP-linked CST (7076)	
β-tubulin	Invitrogen (32-2600)			

2.14 Isolation of BAT mitochondria and respirometry

BAT from the interscapular and axillary regions were combined from individual mice and rinsed in ice-cold buffer B1 (250 mM sucrose, 100 mM KCl, 20 mM K-TES pH 7.2, 0.3 % fatty acid free BSA). BAT mitochondria were isolated by differential centrifugation, essentially as described [85,86]. All isolation steps were performed on ice or at 4 °C. BAT was minced with scissors in buffer B1 and homogenized in a tight fitting Potter homogenizer with a Teflon pestle. The homogenized tissue was filtered through gauze and centrifuged at 8500 g for 10 min. The pellet was resuspended in B1 and centrifuged at 800 g for 10 min, and the resulting supernatant was centrifuged at 8500 g for 10 min to give a crude mitochondrial pellet. The mitochondrial pellet was resuspended in buffer B2 (100 mM KCl, 20 mM K-TES pH 7.2, 1 mM EDTA, 0.6 % fatty acid free BSA) and centrifuged at 8500 g for 10 min. The final pellet was resuspended in 60-70 µL of respiration buffer (125 mM sucrose, 20 mM K-TES pH 7.2, 2 mM $MgCl_2$, 1 mM EDTA, 4 mM KH_2PO_4 0.1 % fatty acid free BSA) and assessed for respiratory activity. An aliquot of mitochondria was frozen at -80 °C for later quantification of protein content and Western blot analysis.

Mitochondrial respiration was performed in an Oroboros Oxygraph-2k with 2 mL of respiration buffer. The isolated mitochondria were added to respiration buffer containing 2 mM malate and 2.5 mM L-carnitine, followed by subsequent additions of 30 µM palmitoyl-CoA, 2 mM GDP, 450 µM ADP, 2 mg/mL oligomycin and FCCP to determine the rate of respiration. The concentration of FCCP was titrated in to a final

concentration of 1 μM, which gave maximal respiration rates. All chemicals were from Sigma Aldrich (Toronto, Canada).

2.15 Immunostaining

Tissue sections were deparaffinized, rehydrated and antigen retrieval was conducted for 5 minutes at high pressure in sodium citrate buffer (pH 6.0) (Cuisinart CPC-600 pressure cooker). Sections were then incubated in 0.5% Triton-X for 30 minutes at room temperature and blocked in 5% Normal Goat Serum for 40 minutes at room temperature. Sections were incubated in a cocktail of primary antibodies (Parkin 1:200 and Tom20 1:50 in block) overnight at 4˚C, followed by a cocktail of appropriate secondary antibodies (1:250) for 2 hours at room temperature. DAPI was used as a counterstain, and all images were collected using a 100x objective using a Nikon 90i Eclipse (Nikon Inc., NY, USA) microscope. Briefly, 5 images were taken per animal by random sampling, and number of Tom20, and co-localized Parkin with Tom20 signals were counted and averaged per animal to give % Tom20 co-localized with Parkin .

CHAPTER III – RESULTS

CHAPTER III – RESULTS

3.1 The inducible adipose tissue-specific AMPK β1β2 knockout mouse (iβ1β2AKO)

In pursuance of the *in vivo* role of AMPK in the metabolic function of BAT and WAT, we generated an inducible genetic knockout mouse model for the AMPK β1 and β2 subunits specifically in adipocytes (iβ1β2AKO) (Figure 1A, Methods**)**. The β subunits were chosen for deletion, as they are required to tether the AMPK αβγ heterotrimer [87]. This specific model was chosen for reasons two-fold: the whole-body deletion of both AMPK β1 and β2 is embryonically lethal and AMPK may play a vital role in the development of adipose tissue [80,88,89]. Immunoblotting shows a reduction of AMPK β1 and β2 in whole adipose tissues but not other metabolic tissues (Figure 1B**)**. Deletion of AMPK β1 and β2 occurred in adipocytes, but not in the stromal vascular fraction (SVC), which is composed of vasculature, macrophages, and other cells [90]. This suggests that residual expression of AMPK in adipose tissue is from non-adipocyte cells (See Appendix). The removal of both AMPK β subunits resulted in subsequent reductions in the phosphorylation of AMPKα T172, and the phosphorylation of its downstream substrate ACC S79, in comparison to total protein levels (Figure 1B). In order to induce the deletion of AMPK β1 and β2 subunits specifically in adipocytes, we treated 7-8 week-old mice, both expressing (iβ1β2AKO) or not expressing (Control) $CreER^{T2}$, with the drug tamoxifen for five consecutive days. Although there was a significant decrease in body weight 8 days after the first administration of tamoxifen (Days 0), all mice recovered from the initial loss in weight by Day 15 (Figure 1C). Furthermore, female

Control and iβ1β2AKO mice, in a room kept between 26 and 28 °C, showed no significant differences in whole-body metabolic parameters of oxygen consumption (VO_2), carbon dioxide production (VCO_2), heat, food intake, water intake, and activity (Figure 1D-I). Altogether, inducing the deletion of both AMPK β subunits was adequate, adipocyte specific, and did not produce an overt metabolic phenotype under basal conditions.

3.2 iβ1β2AKO mice are intolerant to cold

One of the functions of BAT is to preserve body temperature in response to cold by increasing non-shivering thermogenesis [20]. Therefore, we decided to expose female Control and iβ1β2AKO mice to an acute bout of cold stress (4 °C). In order to eliminate all previous adrenergic stimuli, mice were placed at thermoneutrality (30 °C) one week prior to being challenged by cold (Figure 2A). iβ1β2AKO mice were intolerant to cold, as noted by the large reductions in core body temperature (Figure 2B) and interscapular BAT temperature (Figure 2C and D) by 2 hours of 4 °C exposure. Additionally, triglyceride levels of cold exposed-BAT from Control mice were significantly reduced in comparison to thermoneutrality, but this reduction was not seen in iβ1β2AKO mice (Figure 2E). These effects were not due to a deficiency in releasing FFA or glycerol into the bloodstream (Figure 2F and G). Moreover, we found that 2 hours of cold exposure increased levels of phosphorylated AMPKα T172 compared to total AMPKα in the BAT of Control mice, but not in iβ1β2AKO mice (Figure 2H and I). The augmented levels of AMPKα phosphorylation (T172) in Control mice were not paralleled by an increase in

ACC S79 phosphorylation, but there was a trend (Figure 2H and J). Lastly, UCP1 protein content was reduced in iβ1β2AKO mice (Figure 2H and K).

3.3 Adipocyte AMPK is required for the complete induction of UCP1-mediated non-shivering thermogenesis

In order to dissect the cold intolerance effects seen in the iβ1β2AKO mice, we decided to test the ability of Control and iβ1β2AKO mice to acutely induce UCP1-mediated non-shivering thermogenesis by performing infrared thermography (Figure 3A) [77]. In response to the pharmacological activation of β3-Adrenergic Receptors using a single intraperitoneal injection of the highly selective agonist CL-316,243, Control mice showed increases in oxygen consumption (Figure 3B) and interscapular BAT temperature (Figure 3C and D), but this effect was attenuated in iβ1β2AKO mice. Reiterating the findings from the cold exposure experiments, we found no differences in FFA release into the plasma in basal nor CL-316,243 stimulated states (Figure 3E). Furthermore, when treating wildtype (WT) mice with saline or CL-316,243 for 20 minutes before collecting BAT, we observed the activation and phosphorylation of AMPKα (T172) and its downstream target Raptor (S792) (Figure 3F and G).

It has been known for quite some time that AMPK has a role in regulating fatty acid metabolism, specifically in the liver and skeletal muscle [44,91]. One of the mechanisms by which AMPK regulates fatty acid oxidation is through the phosphorylation of acetyl-CoA carboxylase (ACC). This, in turn, inhibits the production of malonyl-CoA from acetyl-CoA, and results in less allosteric inhibition of carnitine palmitoyltransferase 1

(CPT1); increasing β-oxidation [44]. Thus, we decided to test whether the deficits in iβ1β2AKO mice in response to cold and β-adrenergic stimulation were due to this AMPK-ACC pathway by using mice with targeted mutations in the AMPK phosphorylation sites on ACC (ACC1 Ser79-to-Ala and ACC2 Ser212-to-Ala knock-in (ACC DKI, characterized in [54])). In an acute bout of cold exposure (4 °C), ACC DKI mice responded similarly to wildtype (WT) mice, as shown by the maintenance of core body (Figure 4A) and interscapular BAT (Figure 4B and C) temperatures. These conclusions are further supported by the similar increases in oxygen consumption (Figure 4D**)** and top 10% mean surface area temperature of the interscapular region (Figure 4E and F) in WT and ACC DKI mice responding to an acute injection of CL-316,243. These results suggest that the effects seen in iβ1β2AKO mice were not through the AMPK-ACC axis and required further investigation.

3.4 AMPK is important for the metabolic remodeling of adipose tissues in response to β3-adrenergic stimulation

We next tested the adaptive responses of Control and iβ1β2AKO mice to a five-day CL-316,243 challenge (5D CL) (Figure 5A). 5D CL elevated oxygen consumption (Figure 5B), carbon dioxide production (Figure 5C), and resulted in an increase in heat production (Figure 5D) in Control mice, but these effects were abated in iβ1β2AKO mice. It is important to note that these effects were not due to differences in body weight, food intake, water intake, activity levels, nor FFA and glycerol release (Figure 5E-J). Therefore, the differences were attributed to a defect in adipose tissue metabolism and led to more extensive examination.

Since differences were seen in whole-body metabolism, we wanted to test whether these defects were due to disparities in BAT metabolism and markers of mitochondrial content. BAT fatty acid oxidation was significantly elevated in Control mice treated 5D CL in comparison to saline, but this increase was not found in iβ1β2AKO mice (Figure 6A). Additionally, increases in cytochrome *c* oxidase (COX) activity in iβ1β2AKO mice were attenuated in comparison to Control mice (Figure 6B). Furthermore, the content of electron transport chain subunits in BAT of Control and iβ1β2AKO mice, measured using a total OXPHOS antibody, was similar between genotypes under saline conditions, but there was a dampened increase in response to 5D CL in the BAT of iβ1β2AKO mice compared to Control (Figure 6C). Also, the transcriptional co-activator and a master regulator of mitochondrial biogenesis, peroxisome proliferator-activated receptor gamma coactivator 1-alpha (PGC-1α), showed an attenuated response to 5D CL in iβ1β2AKO mice compared to Control, with no alterations in the content of UCP1 (Figure 6D and E).

3.5 Adipocyte AMPK is required for the browning of WAT in response to β3-adrenergic stimulation

Of great therapeutic interest is the potential ability to convert WAT to a phenotype that resembles and functions similarly to BAT through a process termed browning. This process causes an increase in mitochondrial biogenesis in WAT, which allows for more uncoupling of oxidative phosphorylation through UCP1. Thus, the attenuated increases in heat production with 5D CL treatment may have resulted from the impairment of iβ1β2AKO mice to remodel WAT into beige adipose tissue. The iWAT of Control mice

that were treated for five days with CL-316,243 appeared to have a larger presence of multilocular adipocytes compared to iβ1β2AKO mice (Figure 7A). We found no significant differences in iWAT fatty acid oxidation in any genotype or condition, as the basal rates are approximately 10 times lower than that of BAT (Figure 7B), suggesting that BAT is the predominant site for fatty acid oxidation in response to β3-AR activation. Additionally, increases in COX activity in the iWAT of iβ1β2AKO mice were attenuated in comparison to Control mice (Figure 7C). Moreover, the increases in expression of thermogenic/browning and mitochondrial genes (BMRGs) in response to 5D CL were dramatically reduced in iβ1β2AKO mice compared to Control mice, with iWAT Ucp1 mRNA expression levels being approximately 4.4 times higher in Control mice than iβ1β2AKO mice treated 5D CL (Figure 7D and E). To add, the increase in content of electron transport chain subunits in iWAT of Control and iβ1β2AKO mice was dampened in response to 5D CL in iβ1β2AKO mice compared to Control (Figure 7F). More importantly, there was an attenuated response to 5D CL in iβ1β2AKO mice compared to Control with regards to UCP1 content; being 3.3 times higher in Control mice versus iβ1β2AKO mice treated 5D CL (Figure 7G).

3.6 AMPK in adipocytes is crucial for the maintenance of mitochondrial morphology and function

Considering that the deficits in the activation of BAT in iβ1β2AKO mice in response to cold exposure and the β3-adrenergic receptor agonist treatment were not due to the AMPK-ACC pathway, we examined mitochondrial morphology and function.

Transmission electron microscopy revealed an altered mitochondrial structure with greater cristae disruption in iβ1β2AKO mice (Figure 8A and B). This observation was despite similar total number of mitochondria per micrograph (Figure 8C). To further support AMPK's role in maintaining the integrity of mitochondria in adipocytes, isolated mitochondria from iβ1β2AKO mice showed significantly lower respiration rates in the presence of substrates palmitoyl-CoA, GDP, and oligomycin, with FCCP rates being reduced (p=0.06) (Figure 8D).

Knowing that BAT is a highly metabolic tissue and that there is constant turnover of cells and organelles, we decided to investigate the housekeeping mechanisms of macroautophagy (hereafter termed autophagy) and mitophagy in Control and iβ1β2AKO mice. The role of AMPK in autophagy is very complex and still not fully understood. Depending on the cell type and metabolic state, AMPK may have very distinct effects with regards to the autophagy process [92,93]. For some time now, AMPK has been known to induce autophagy in skeletal muscle, but whether it promotes the recycling of cellular contents within BAT is unknown [65]. Here, we observed that the loss of AMPK in brown adipocytes reduced the amount of phosphorylated unc-like autophagy activating kinase 1 (ULK1) on Ser555, a critical inducer of autophagy (Figure 9A). This resulted in reduced lipidation of the crucial phagophore formation protein LC3B (LC3B-II/LC3B-I) in iβ1β2AKO mice, thus compromising the formation of phagophores for autophagy (Figure 9B). Additionally, the accumulation of the adaptor protein p62 (also known as SQSTM1) was increased in iβ1β2AKO mice compared to Control mice (Figure 9C). To further corroborate the results, levels of LC3B were reduced (p=0.08) and amounts of p62 were

increased in isolated mitochondria of BAT in iβ1β2AKO mice compared to Control mice (Figure 9D and E). Lastly, since autophagy is involved in the process of remodelling a cell, we investigated whether the basal defects in BAT mitophagy would extend to a chronic remodelling challenge. Immunostaining for mitochondrial protein Tom20 and Parkin, a protein that tags dysfunctional mitochondria for degradation, showed more co-localization in response to CL-316,243 for five days in Control mice compared to iβ1β2AKO mice (Figure 9F). These data suggest that adipocyte AMPK is important in the maintenance of mitochondrial morphology and function.

CHAPTER IV – FIGURES

CHAPTER IV – FIGURES

Figure 1.

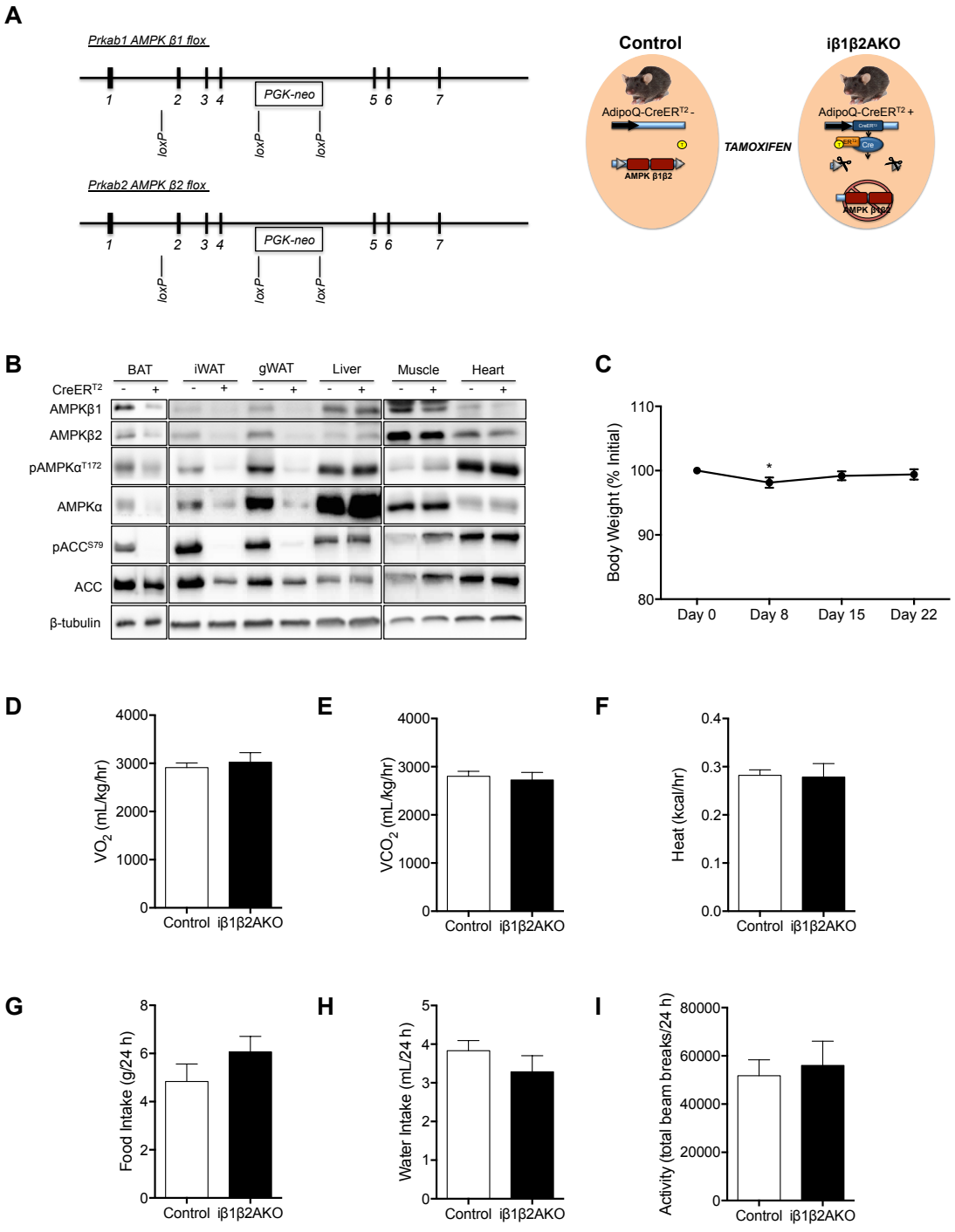

FIGURE 1. THE INDUCIBLE ADIPOSE TISSUE-SPECIFIC AMPK β1β2 KNOCKOUT MODEL (iβ1β2AKO) Illustration of targeting constructs for AMPK Prkab1 and Prkab2 (adapted from [80]), as well as the tamoxifen/AdipoQCreER^{T2}-inducible system (A). BAT, inguinal WAT, gonadal WAT, Liver, Muscle, and Heart were immunoblotted using the indicated antibodies to show efficient and tissue-specific deletion of adipocyte AMPK β1β2 by tamoxifen in iβ1β2AKO mice (CreER^{T2} +) in comparison to Control (CreER^{T2} -) (B). Tamoxifen effects on body weight of all treated mice undergoing daily oral gavage of tamoxifen (Day 0-Day 5) and recovery period (C) (n = 19). Metabolic parameters of oxygen consumption (D), carbon dioxide production (E), heat (F), food and water intake (G and H) and activity (I) of female Control and iβ1β2AKO mice in a room kept between 26-28 °C (n = 6-7 per group). * $p < 0.05$ indicates an effect of tamoxifen on body weight, determined via repeated-measures one-way ANOVA and bonferroni *post hoc*.

Figure 2.

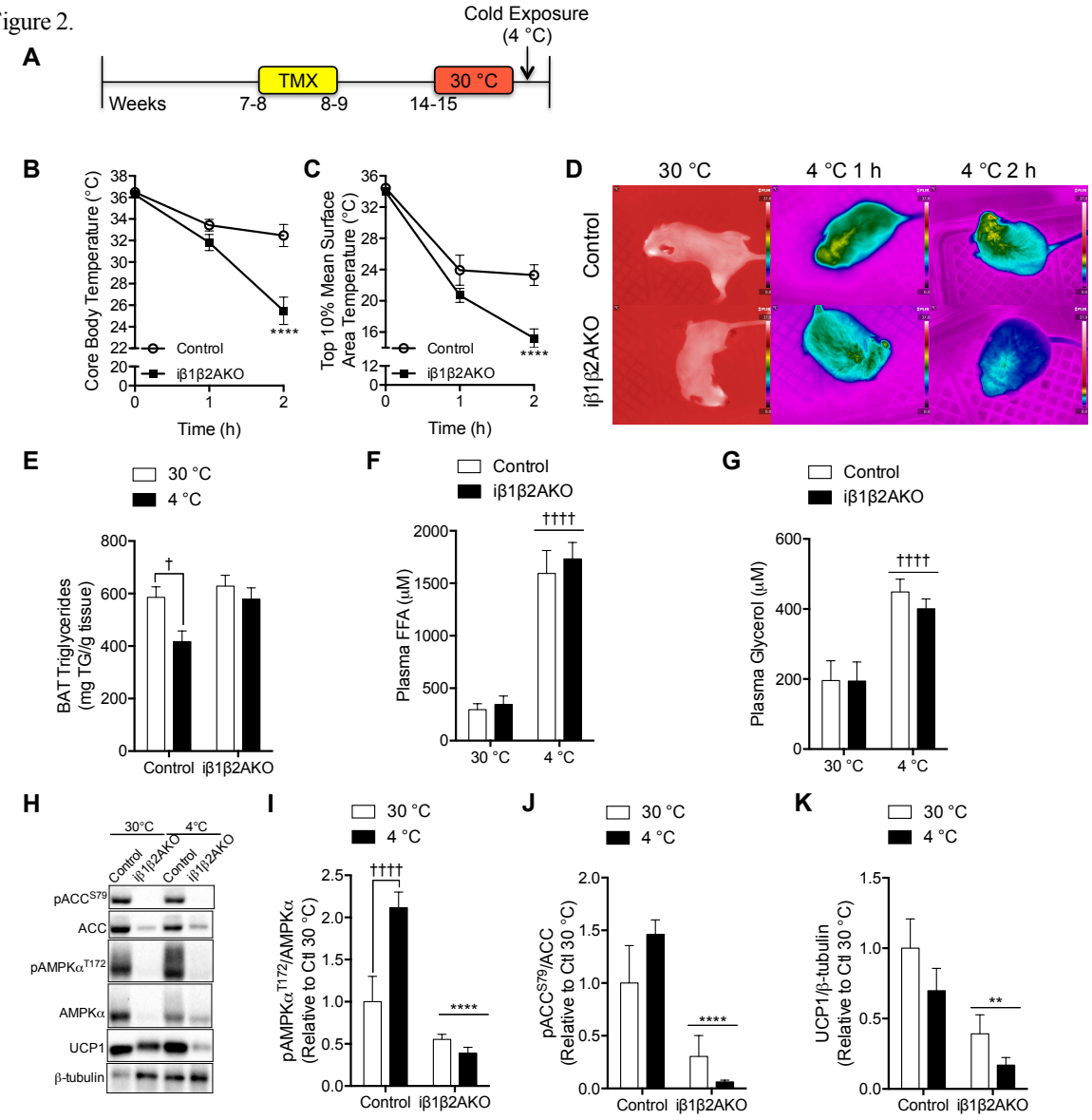

FIGURE 2. iβ1β2AKO MICE ARE INTOLERANT TO COLD

Timeline for tamoxifen (TMX) administration and cold exposure of female Control and iβ1β2AKO mice (A). (B-D) Core body temperature (B), interscapular BAT surface area temperature (C), and representative thermal images (D) of Control and iβ1β2AKO mice at thermoneutrality (30 °C) and cold exposed (4 °C) for 1 and 2 hours (n = 6-9 per group). (E-G) BAT triglyceride (E), plasma free fatty acids (F), and plasma glycerol (G) content

in Control and iβ1β2AKO mice exposed to cold for 3 h (n = 4-7 per group). (H-K) Phosphorylated (T172 and S79) over total AMPKα (H and I) and ACC (H and J), respectively, and total UCP1 (K) protein in BAT of Control and iβ1β2AKO mice in response to 3 h cold compared to thermoneutral group (n = 4-6 per group). ** $p < 0.01$ and **** $p < 0.0001$ indicates a genotype difference, and † $p < 0.05$ and †††† $p < 0.0001$ indicates a treatment effect within genotype determined via 2-way ANOVA and Bonferroni *post hoc*.

Figure 3.

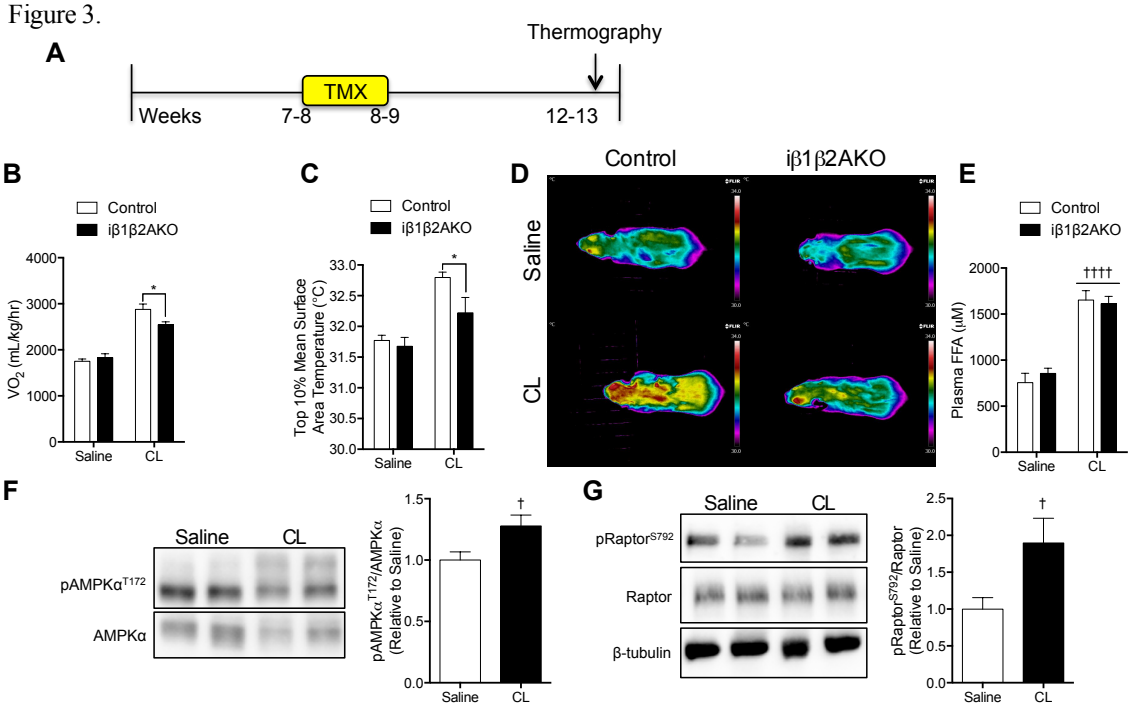

FIGURE 3. ADIPOCYTE AMPK IS REQUIRED FOR THE COMPLETE INDUCTION OF UCP1-MEDIATED NON-SHIVERING THERMOGENESIS (A-D) Oxygen consumption (VO_2) (A), interscapular BAT surface area temperature (B), representative thermal images (C), and plasma free fatty acids (D) in female Control and iβ1β2AKO mice responding to an acute injection of saline or the β3-adrenergic receptor agonist CL-316,243 (CL) (n = 8 per group). Phosphorylated (T172 and S792) over total AMPKα (F) and Raptor (G), respectively in wildtype (WT) mice treated with 0.033 nmol/g body weight of CL-316,243 or an equal volume of saline (n = 6 per group). * $p < 0.05$ indicates a genotype difference, and †††† $p < 0.0001$ indicates a treatment effect determined via repeated-measures 2-way ANOVA and Bonferroni *post hoc*. † $p < 0.05$ indicates a treatment effect determined via Student's *t*-test.

Figure 4.

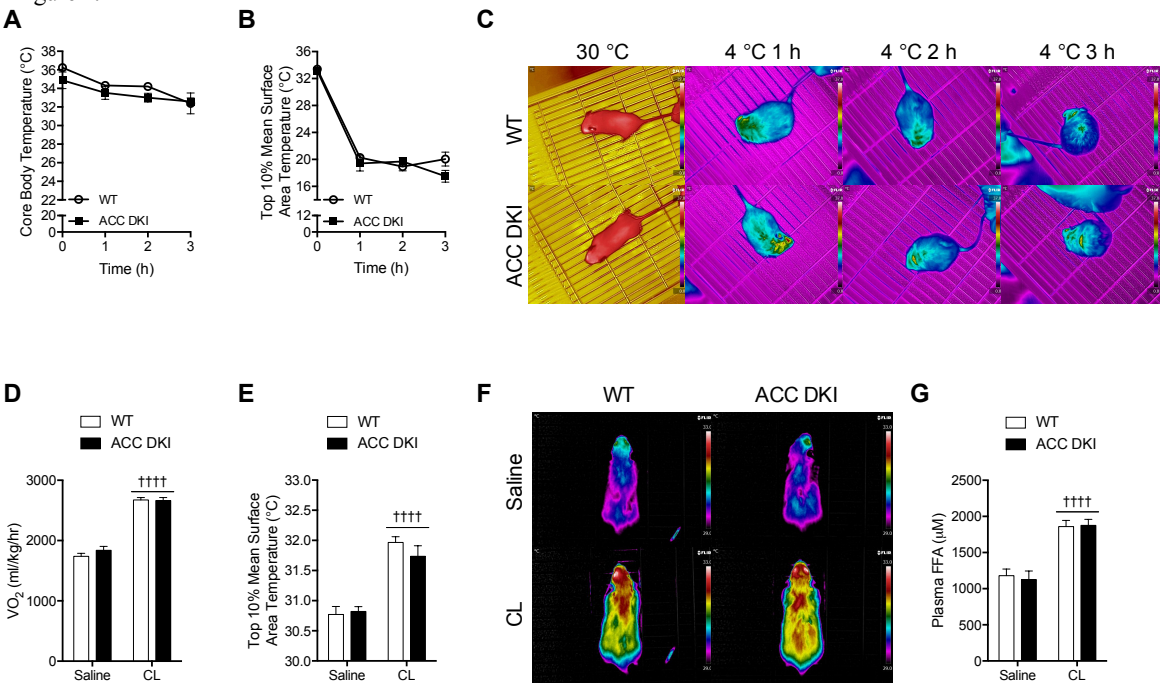

FIGURE 4. AMPK INHIBITION OF ACC IS NOT REQUIRED FOR THE INDUCTION OF UCP1-MEDIATED NON-SHIVERING THERMOGENESIS (A-C) Core body temperature (A), interscapular BAT surface area temperature (B), and representative thermal images (C) of WT and ACC DKI mice at thermoneutrality (30 °C) and cold exposed (4 °C) for 1 to 3 hours (n = 5-6 per group). (D-G) Oxygen consumption (VO_2) (D), interscapular BAT surface area temperature (E), representative thermal images (F), and plasma free fatty acids (G) in female WT and ACC DKI mice responding to an acute injection of saline or the β3-adrenergic receptor agonist CL-316,243 (CL) (n = 17-19 per group). †††† $p < 0.0001$ indicates a treatment effect determined via repeated-measures 2-way ANOVA and Bonferroni *post hoc*.

Figure 5.

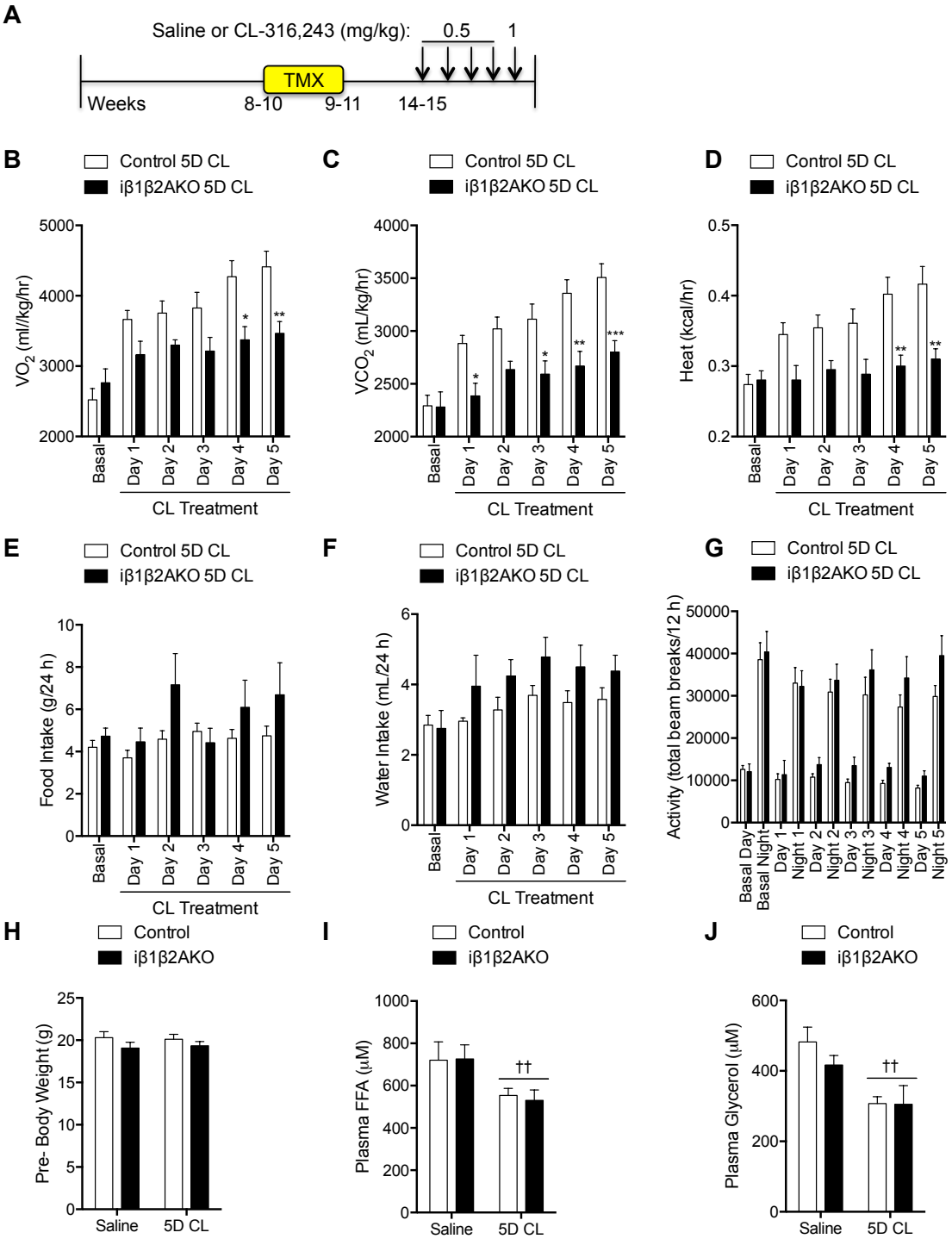
A
Saline or CL-316,243 (mg/kg):
0.5
1
TMX
Weeks
8-10
9-11
14-15
B
Control 5D CL
iβ1β2AKO 5D CL
VO2 (ml/kg/hr)
Basal
Day 1
Day 2
Day 3
Day 4
Day 5
CL Treatment
C
Control 5D CL
iβ1β2AKO 5D CL
VCO2 (mL/kg/hr)
CL Treatment
D
Control 5D CL
iβ1β2AKO 5D CL
Heat (kcal/hr)
CL Treatment
E
Control 5D CL
iβ1β2AKO 5D CL
Food Intake (g/24 h)
CL Treatment
F
Control 5D CL
iβ1β2AKO 5D CL
Water Intake (mL/24 h)
CL Treatment
G
Control 5D CL
iβ1β2AKO 5D CL
Activity (total beam breaks/12 h)
Basal Day
Basal Night
Day 1
Night 1
Day 2
Night 2
Day 3
Night 3
Day 4
Night 4
Day 5
Night 5
H
Control
iβ1β2AKO
Pre- Body Weight (g)
Saline
5D CL
I
Control
iβ1β2AKO
Plasma FFA (μM)
††
Saline
5D CL
J
Control
iβ1β2AKO
Plasma Glycerol (μM)
††
Saline
5D CL

FIGURE 5. ADIPOCYTE AMPK IS IMPORTANT FOR WHOLE-BODY METABOLIC REMODELLING IN RESPONSE TO β3-AR ACTIVATION Timeline for tamoxifen (TMX) administration and five-day CL-316,243 (5D CL) treatment of female Control and iβ1β2AKO mice (A). (B-G) Whole-body metabolic parameters of oxygen consumption (B), carbon dioxide production (C), heat (D), food and water intake (E and F) and activity (G) basally or on days indicated (6 hours post-CL treatment for VO_2, VCO_2, and heat) in Control and iβ1β2AKO mice (n = 6-9 per group). Body weights of groups before experiment (H), plasma free fatty acids (I) and plasma glycerols (J) of Control and iβ1β2AKO mice treated with saline or CL for five days (n = 8-11 per group). * $p < 0.05$, ** $p < 0.01$ and *** $p < 0.001$ indicates a genotype difference, and †† $p < 0.01$ indicates a treatment effect determined via 2-way ANOVA and Bonferroni *post hoc*.

Figure 6.

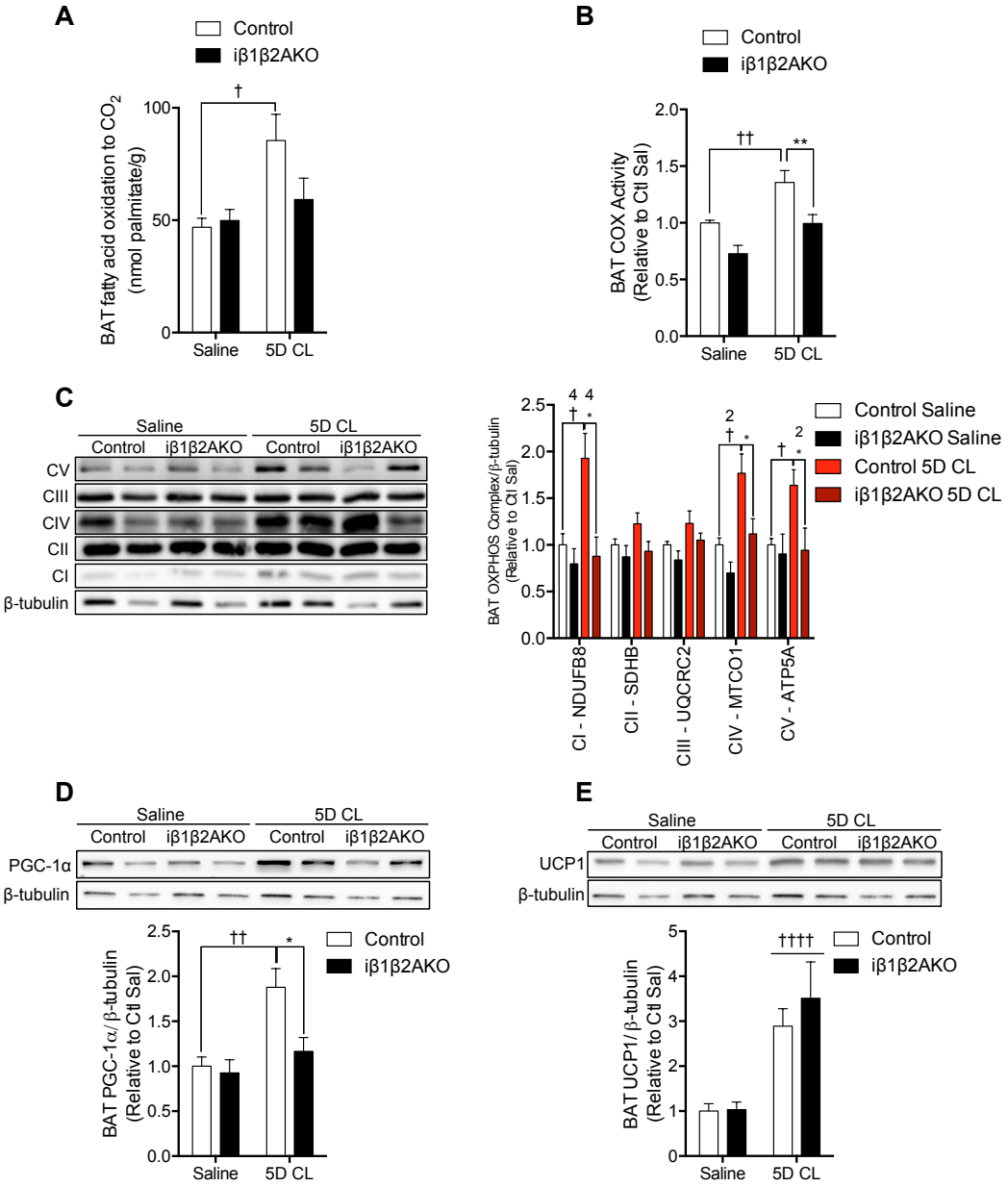

FIGURE 6. ADIPOCYTE AMPK IS IMPORTANT FOR THE METABOLIC REMODELLING OF BAT IN RESPONSE TO β3-AR ACTIVATION Fatty acid oxidation (A) (n = 5-7 per group) and cytochrome *c* oxidase activity (B) (n = 8-10 per group) in BAT of female Control and iβ1β2AKO mice treated with saline or CL for five

consecutive days. Representative immunoblotting with quantification of OXPHOS subunits (C) (n = 7-9 per group), PGC-1α (D) (n = 5-7 per group), and UCP1 (E) (n = 8-9 per group) in BAT of Control and iβ1β2AKO mice treated with saline or CL for five consecutive days in a room kept between 26 and 28 °C. * $p < 0.05$, ** $p < 0.01$, *** $p < 0.001$ and **** $p < 0.0001$ indicates a genotype difference, and † $p < 0.05$, †† $p < 0.01$ and †††† $p < 0.0001$ indicates a treatment effect determined via 2-way ANOVA and Bonferroni *post hoc*.

Figure 7.

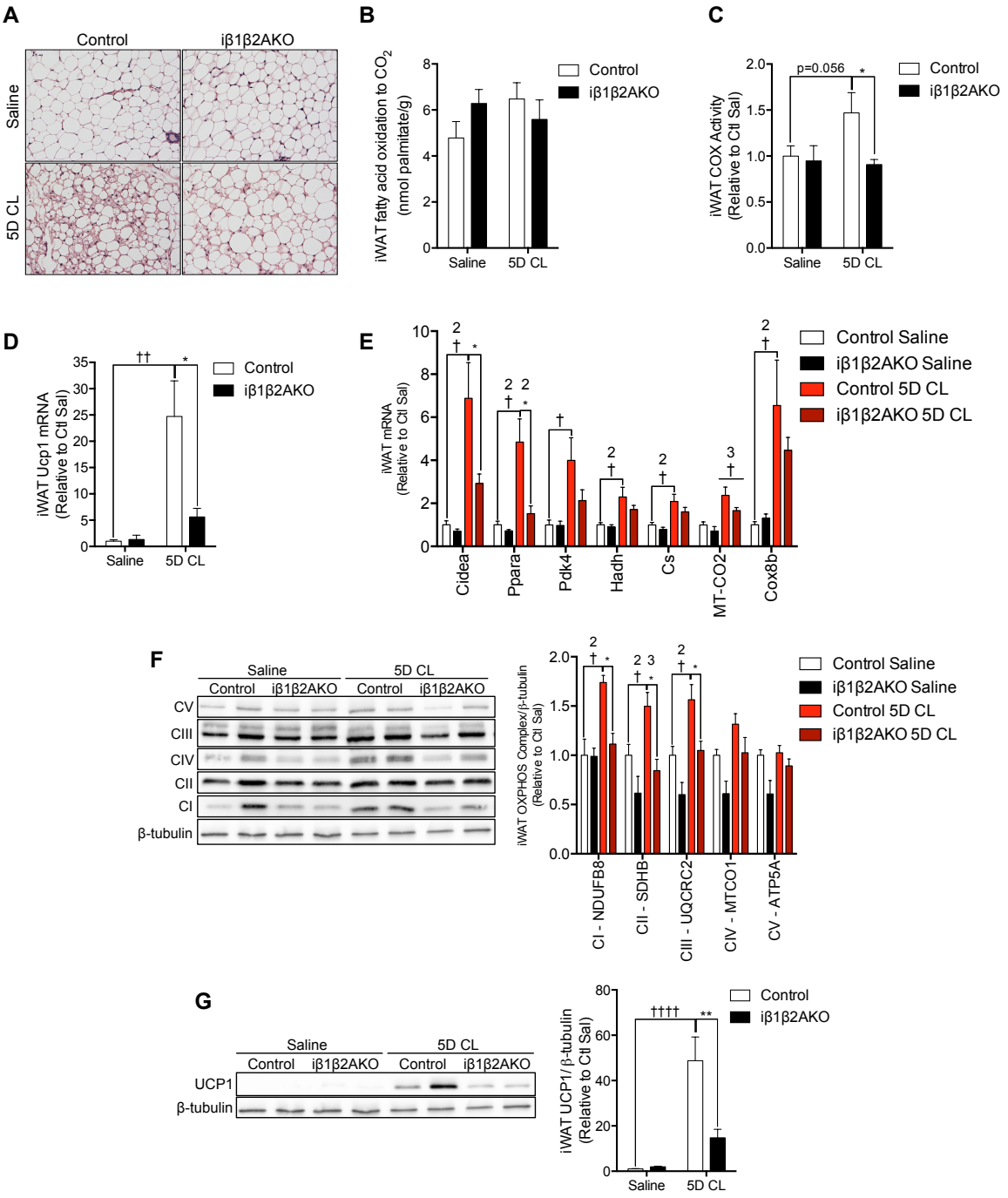

FIGURE 7. ADIPOCYTE AMPK IS IMPORTANT FOR THE BROWNING OF WAT IN RESPONSE TO β3-AR ACTIVATION Representative iWAT haemotoxylin and eosin images of Control and iβ1β2AKO mice treated with saline or CL for 5 days (A). Fatty

acid oxidation (B) (n = 5-7 per group) and cytochrome *c* oxidase activity (C) (n = 8-10 per group) in iWAT of female Control and iβ1β2AKO mice treated with saline or CL for five consecutive days. iWAT mRNA of Ucp1 (D) and indicated thermogenic genes (E) of Control and iβ1β2AKO mice treated with saline or CL for 5 days (n = 8-11 per group). Representative immunoblotting with quantification of OXPHOS subunits (F) (n = 4-8 per group) and UCP1 (G) (n = 7-10 per group) in iWAT of Control and iβ1β2AKO mice treated with saline or CL for five consecutive days in a room kept between 26 and 28 °C. * $p < 0.05$, ** $p < 0.01$ and *** $p < 0.001$ indicates a genotype difference, and † $p < 0.05$, †† $p < 0.01$ and †††† $p < 0.0001$ indicates a treatment effect determined via 2-way ANOVA and Bonferroni *post hoc*.

Figure 8.

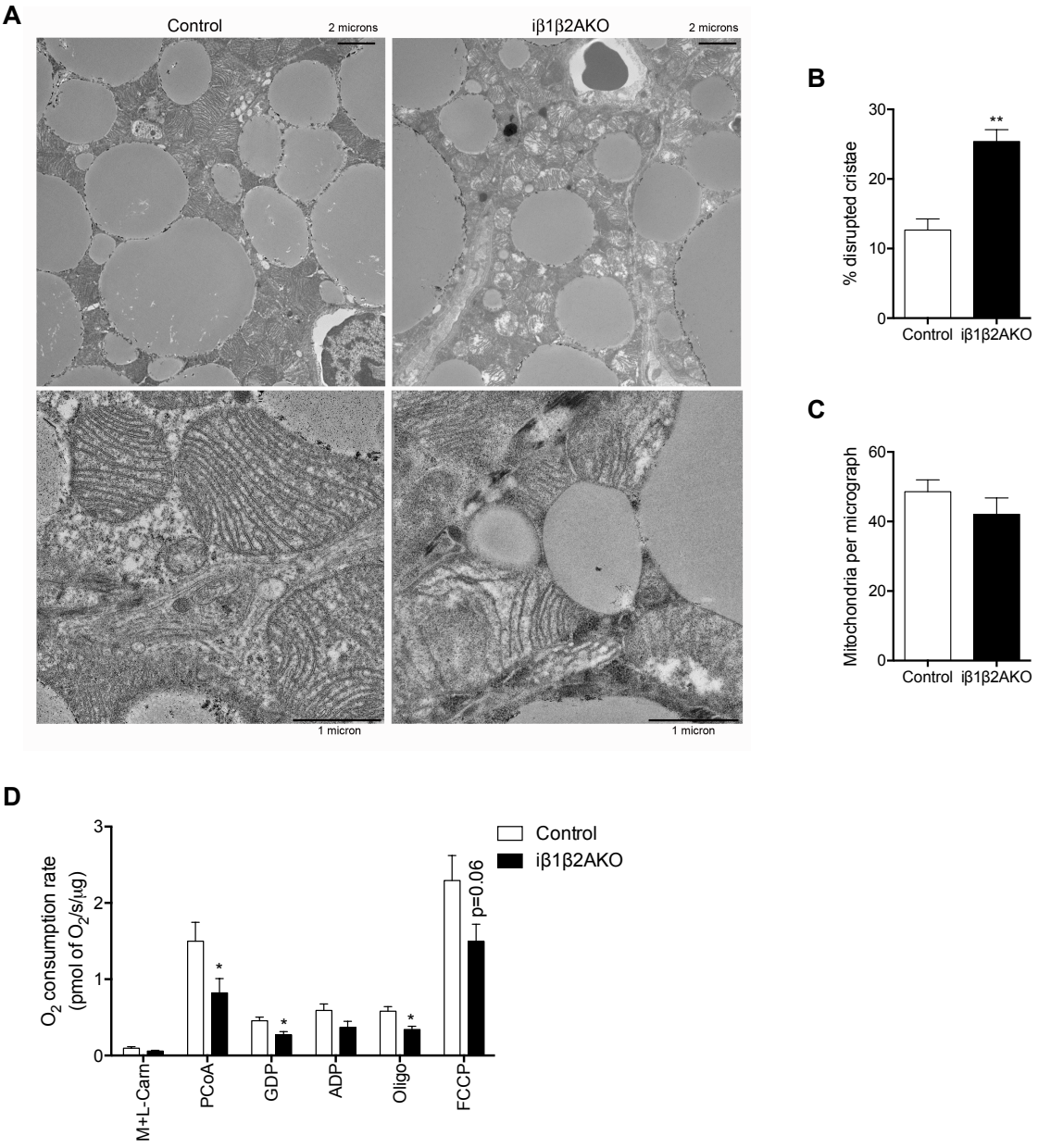

FIGURE 8. AMPK IN ADIPOCYTES IS CRUCIAL FOR THE MAINTENANCE OF MITOCHONDRIAL MORPHOLOGY AND FUNCTION IN BAT (A-C) Representative transmission electron micrographs of mitochondria at two magnifications (A), images quantified for % disrupted cristae (B) and mitochondria per micrograph (C) in BAT of

Control and iβ1β2AKO mice (n = 3-4 per group). Isolated BAT mitochondria respiration with malate and L-carnitine (M + L-Carn: 2 mM and 2.5 mM), palmitoyl CoA (PCoA: 30 μM), GDP (2 mM), ADP (450 μM), oligomycin (Oligo: 2 mg/mL), and FCCP (1 μM) (n = 7 isolations per genotype). * $p < 0.05$ and ** $p < 0.01$ indicates a genotype difference measured via Student's *t*-test.

Figure 9.

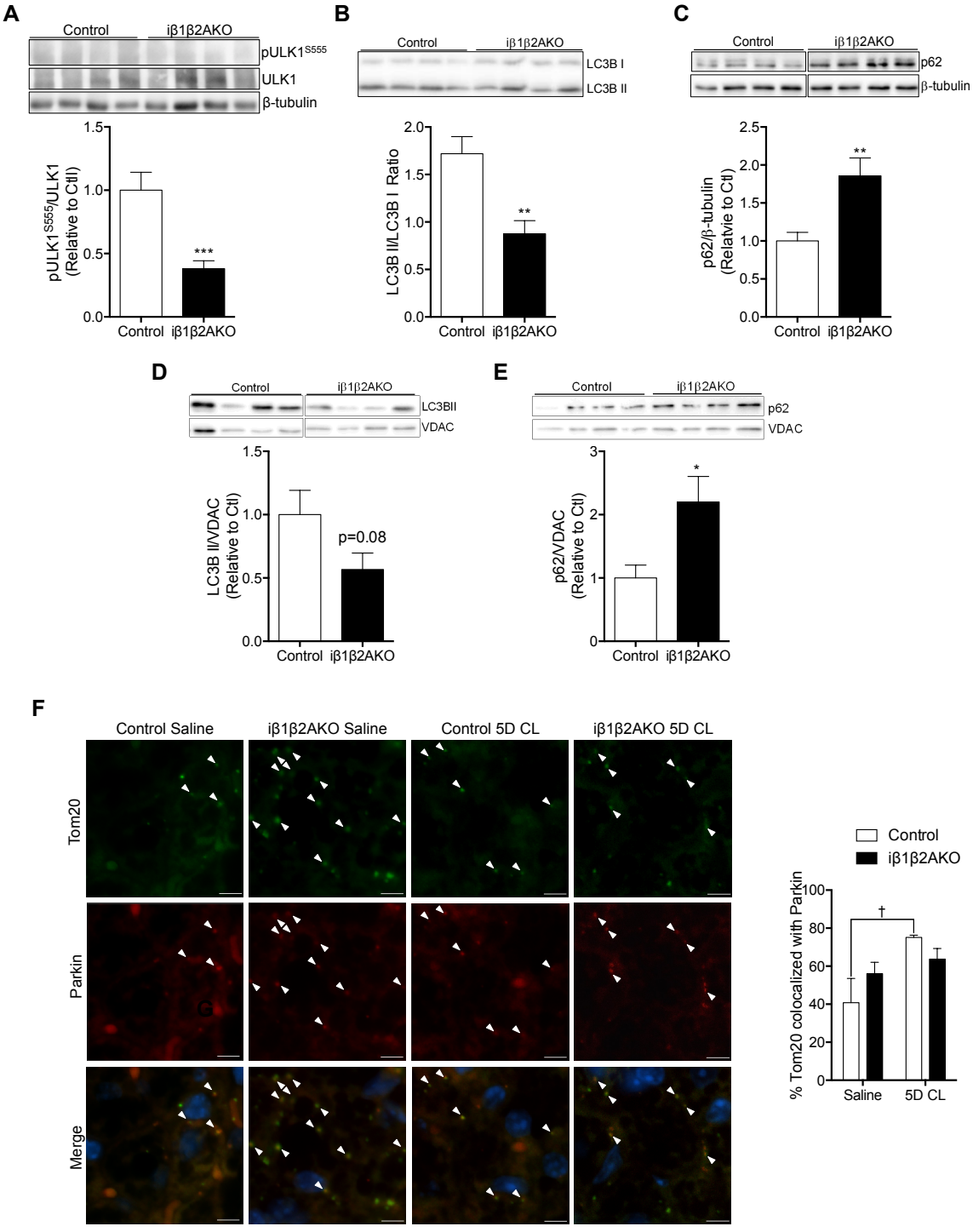
A
Control
iβ1β2AKO
pULK1S555
ULK1
β-tubulin
pULK1S555/ULK1 (Relative to Ctl)
***
Control iβ1β2AKO
B
Control
iβ1β2AKO
LC3B I
LC3B II
LC3B II/LC3B I Ratio
**
Control iβ1β2AKO
C
Control
iβ1β2AKO
p62
β-tubulin
p62/β-tubulin (Relatvie to Ctl)
**
Control iβ1β2AKO
D
Control
iβ1β2AKO
LC3BII
VDAC
LC3B II/VDAC (Relative to Ctl)
p=0.08
Control iβ1β2AKO
E
Control
iβ1β2AKO
p62
VDAC
p62/VDAC (Relative to Ctl)
*
Control iβ1β2AKO
F
Control Saline
iβ1β2AKO Saline
Control 5D CL
iβ1β2AKO 5D CL
Tom20
Parkin
Merge
Control
iβ1β2AKO
% Tom20 colocalized with Parkin
†
Saline
5D CL

FIGURE 9. ADIPOCYTE AMPK IS INVOLVED IN BAT AUTOPHAGY AND MITOPHAGY (A-E) Representative immunoblotting with quantification of whole-tissue BAT phosphorylated (S555) over total ULK1 (A) (n = 11-12 per genotype), LC3BII over LC3BI ratio (B) and total p62 (C) (n = 6-7 per genotype), and isolated BAT mitochondria LC3BII (D) and p62 (E) (n = 6-7 per genotype). Immunostaining of Tom20, Parkin, and DAPI (F) from female Control and iβ1β2AKO mice treated with saline or CL for five consecutive days (n= 5-6 per genotype). * $p < 0.05$ ** $p < 0.01$ and *** $p < 0.001$ indicates a genotype difference measured via Student's *t*-test, and † $p < 0.05$ indicates a treatment effect determined via 2-way ANOVA and Bonferroni *post hoc.*

CHAPTER V – DISCUSSION AND FUTURE DIRECTIONS

CHAPTER V – DISCUSSION AND FUTURE DIRECTIONS

5.1 Discussion

With the prevalence of obesity on the rise, it is of paramount importance to generate new treatment tactics that can help patients lose adiposity and reduce the risk for the development of non-communicable diseases. Treatments that help patients initially lose fat mass, as well as aid in keeping the weight off by combatting the phenomenon of "metabolic adaptation"; whereby adaptive thermogenesis is reduced following the physiological implications to perceived starvation, are of immense interest [94]. Current modalities of exercise and diet are effective, but patients' compliance to programs accounting for the principle of diminishing returns is either low, or dwindles over time and results in weight regain [95]. BAT activity is reduced in obese adult humans, thus, understanding the pathways that regulate the activity of BAT, specifically those that reduce its activity in obesity, is of immense interest to forego metabolic complications [29]. With recent observations that AMPK activity in BAT is increased with cold exposure, we decided to investigate the role of AMPK in the metabolic function of brown and beige adipose tissue by creating an inducible, adipose tissue specific knockout model (iβ1β2AKO) [74]. Here, we report that the deletion of AMPK in adipocytes *in vivo* results in the intolerance to cold exposure, the reduction of UCP1-mediated thermogenesis and thermogenic reprogramming in response to β3-AR activation, and a loss of mitochondrial integrity due to a defect in autophagic signaling.

The deletion of AMPK in adipocytes lead to cold-intolerance, and the inability to increase oxygen consumption and interscapular surface area temperature in response to

the β3-AR agonist CL-316,243. We investigated the acute effects of β3-AR stimulation (20 mins CL-316,243) and cold exposure (3 hrs) and observed increases in AMPK activation in BAT of Control, but not iβ1β2AKO mice. These findings are in accordance with previous reports [75,96,97], but contrast the findings found by Mulligan and colleagues in 2007 who found that AMPK activity in the BAT of mice was unchanged after 2 hours of cold exposure (4 °C) [74]. One reason why Mulligan may not have observed an increase in AMPK activity is because tissues were collected after 2 hours, rather than 3 hours as we performed in our study. As such, differences in timing could mask the increases, as there is a possibility that AMPK activity transiently increases over time. While the exact mechanism by which AMPK is activated in response to these conditions is not fully understood, evidence suggests that lipolysis is important [98,99]. Therefore, it is possible that AMPK is activated in BAT through direct interactions with long-chain fatty acyl-CoA's or via increases in the [AMP]/[ADP]: [ATP] ratio as a result of mitochondrial uncoupling or futile cycling between lipolysis and lipogenesis [97,98,100]. Future studies investigating these possibilities will be important to determine how best to activate AMPK in BAT.

A recent study by Lee and colleagues shows that fatty acid oxidation is required for cold-induced thermogenesis in BAT [101]. This group discovered that mice with a loss of adipose tissue CPT2 ($CPT2^{A-/-}$), an obligate step for long-chain fatty acid oxidation, were intolerant to cold and had attenuations in agonist-induced thermogenic gene expression similar to our findings. Using mice with targeted mutations in the AMPK phosphorylation sites on ACC (ACC1 Ser79-to-Ala and ACC2 Ser212-to-Ala knock-in (ACC DKI)), our lab has recently shown that, in liver and resting skeletal muscle, AMPK

increases fatty acid oxidation through phosphorylation of ACC, which subsequently reduces the concentration of malonyl-CoA and relieves allosteric inhibition of CPT1 [54,91]. This led us to examine the effects of β-adrenergic signaling on acute fatty acid oxidation through AMPK-mediated inhibition of ACC in BAT. Surprisingly, no differences were found in cold tolerance and CL-316,243-induced increases in oxygen consumption and interscapular mean surface area temperature between wildtype and ACC DKI mice, suggesting that AMPK's acute role in brown and beige adipose tissue function is not through the AMPK-ACC axis.

We subsequently investigated the role of AMPK in mitochondrial biogenesis within the BAT and WAT of Control and iβ1β2AKO mice. We report that adipocyte AMPK, in both BAT and WAT, does not mediate basal levels of mitochondrial content, which is in contrast to the findings in AMPK muscle-specific null mice (AMPK β1β2MKO) [80]. This may be due to the nature of the AMPK β1β2MKO model, whereby a lifelong absence of muscle AMPK may lead to a more dramatic phenotype because of an inadequate developmental program. It is also plausible that these two opposing findings shed light on the chronology of events; where a defect of mitophagy may come before a discrepancy in mitochondrial content, and that in a condition of aging, this defect in mitophagy leads to reductions in mitochondrial quality as well as content [93]. However, in response to β3-adrenergic activation, adipocyte AMPK mediates the induction of mitochondrial biogenesis in BAT and WAT, as indicated by increases in cytochrome *c* oxidase activity, the mRNA expression of mitochondrial markers in iWAT, and elevated electron transport chain (OXPHOS) content of Control but not iβ1β2AKO mice. These

increases in markers of mitochondrial biogenesis corresponded with the induction of PGC-1α in Control but not iβ1β2AKO mice, suggesting that the AMPK-PGC-1α axis is required for stimulating mitochondrial biogenesis in adipose tissue.

To the best of our knowledge, we are the first to use a TEM direct detection camera (Gatan K2 Summit) for the visualization of BAT mitochondria [82]. Given the much greater resolution of this camera, this method allowed us to observe that BAT mitochondria of iβ1β2AKO mice had altered ultra-structures within the lipid bilayer of the crista. AMPK may regulate mitochondrial quality through the phosphorylation of a protein called mitochondrial fission factor (MFF) [102]. The facilitation of mitochondrial fission can promote mitophagy to remove damaged mitochondrial structures and maintain a healthy mitochondrial pool [103]. In further experiments not shown in this thesis, we show that the lack of AMPK in BAT adipocytes does not result in reduced phosphorylation of MFF at S129 in response to acute cold, suggesting that, in BAT, alternative kinases are able to maintain phosphorylation of this substrate and that AMPK is not vital for maintaining mitochondrial fission.

However, consistent with the defects in mitochondrial structure we observed abnormalities in autophagic signaling that included reduced activating phosphorylation of the autophagy-initiating protein ULK1, reduced autophagosomal activation as indicated by the LC3BII/LC3BI ratio, and accumulation of the adaptor protein p62. The direct assessment of LC3BII and an increased accumulation of p62 was also observed in isolated mitochondria from BAT, suggesting that mitochondrial specific autophagy (mitophagy) was impaired. Additionally, there was increased co-localization of the

mitochondrial-specific adaptor protein Parkin with the OMM protein Tom20, in response to chronic β3-adrenergic stimulation in Control but not iβ1β2AKO mice. Taken together, the defective autophagy/mitophagy signaling seen in BAT of iβ1β2AKO mice could be a reason why there is altered mitochondrial morphology and function, which contributes to the impairments in the metabolic function of these tissues. Our findings are analogous to a recent study showing that the ablation of adipocyte-specific p62 *in vivo* results in an impaired ability to induce mitochondrial biogenesis and thermogenesis following β3-adrenergic receptor stimulation [104]. These data suggest that AMPK in adipocytes is vital to maintain autophagic activity through proteins such as ULK1 and p62 [105]. Thus, AMPK integrates environmental and pharmacological cues to regulate a fine-tuned mitochondrial network through the processes of mitophagy and ensuing biogenesis to promote BAT activity and the browning of WAT.

Cold and β3-AR agonists have previously been shown to increase the metabolic activity of BAT in humans [106–108]. This results in an increase in energy expenditure and also improves insulin sensitivity. Unfortunately, with the discomfort and inconvenience of short-term cold exposure and the side effect of tachycardia in β3-AR agonists that are not yet selective enough and cause off-target effects in humans, there will be resistance to implementing these therapies in the near future [108]. Thus, at this time, utilizing these methods in rodent models as tools for the discovery of new therapeutic targets seems appropriate. Here, we identify adipocyte AMPK as a potential therapeutic target to increase energy expenditure. It has been reported that AMPK is reduced in the adipose tissue of diabetic patients, thus the tissue-specific activation or reinstatement to normal

levels may be of significance [109]. Caution must be exercised when attempting to develop potent AMPK activators, as a recent report identified negative consequences of chronic central AMPK activation; whereby hyperphagia prevailed over the favorable peripheral effects of AMPK activation [110]. These findings highlight the opposing roles that AMPK has in different tissues; where central AMPK activation increases food intake and reduces SNS activity, while peripheral AMPK activation leads to the activation of catabolic processes [44,53,111]. Knowing that general AMPK activators such as metformin and salicylate are well tolerated by humans, the development of an AMPK activator that specifically targets brown and beige adipose tissue merits consideration [56,112].

5.2 Limitations

Although efforts were made to conduct this research in as comprehensive a manner as possible, there were limitations to our experiments. The most evident limitation is that all cold or β3-adrenergic challenges were performed in female Control and iβ1β2AKO mice and we did not control for what stage of the estrous cycle the mice were in. Though it has been proven, in rats, that sex-dependent differences exist with regards to brown adipose tissue thermogenic features, further experiments (see Appendix Figure 1) show similar cold intolerance in male iβ1β2AKO mice from 23 °C to 4 °C [113,114]. In my opinion, the results we have found in female mice would probably be quite similar in male mice regarding the activation of BAT and the browning of WAT in response to the β3-adrenergic receptor agonist CL-316,243.

As with all tissue-selective genetic mouse models, the specificity of the Cre-promoter is very important. We used a tamoxifen-sensitive Cre recombinase system under

the control of the adiponectin promoter to delete AMPK in adipocytes and showed that, in contrast to the aP2-Cre promoter, there was no effect on AMPK activity in the SVC fraction (See Appendix Figure 2) or other metabolic organs critical for regulating insulin sensitivity (liver and muscle). However, we did not analyze all tissues and, as such, AMPK activity may have been altered in other tissues which were not studied. For example, there is literature that suggests that adiponectin may be expressed at low levels in the brain, which could affect some of our results [115]. Though, if AMPK was lower in the brain, it would be expected to increase BAT activity, not reduce it as we observed in our mice [116]. Thus, it seems unlikely that this could have directly contributed to our results. While we have used the most specific and efficient model to delete AMPK in adipose tissue available at this time, we appreciate that there is potential for some non-specificity to adipose tissue and/or secondary effects from tamoxifen treatment that could have contributed to our findings [79,117–119].

5.3 Future directions

The development of the novel, inducible and tissue-specific iβ1β2AKO mouse model has led to many new questions. First, recent studies have indicated that fatty acid synthesis (lipogenesis) may be important for the browning of white adipose tissue [79,120]. We have found that AMPK is required for the browning of white adipose tissue, but the mechanism mediating these effects was not further interrogated. Since AMPK inhibits fatty acid synthesis through the phosphorylation of ACC, an interesting avenue of further research will be to investigate whether AMPK-mediated phosphorylation of ACC is important for the metabolic reprogramming of BAT and WAT in response to chronic β-

adrenergic stimuli. Subjecting wildtype and ACC DKI mice to five days of saline or CL-316,243 treatment would allow for us to observe whether whole-body metabolic parameters, as well as morphology, fatty acid oxidation, mitochondrial content, thermogenic gene expression, and UCP1 protein of BAT and WAT are regulated through AMPK phosphorylation of ACC and the subsequent inhibition of fatty acid synthesis. A downfall of this study would be that the ACC DKI model is not adipose tissue-specific.

Secondly, the mechanism for AMPK activation in an acute condition of β-adrenergic signaling remains elusive. It is speculated that the effects of lipolysis result in a change in the [AMP]/[ADP]: [ATP] ratio, in turn, leading to the activation of AMPK [98]. Immunoblotting for phosphorylated over total AMPKα (T172) and ACC (S79) in BAT of adipocyte-specific ATGL (rate-limiting enzyme for lipolysis) knockout mice treated acutely with CL-316,243 could indicate whether lipolysis is required for the activation of AMPK in response to β3-adrenergic stimuli.

On a different note, a more thorough examination of the role of AMPK in autophagy/mitophagy in BAT should ensue. Autophagy/mitophagy is a very active process, thus, interpreting it as such would be optimal. Following specific guidelines for the use and interpretation of assays for monitoring autophagy/mitophagy, we would treat Control and iβ1β2AKO mice with saline or the microtubule-destabilizer colchicine (0.4 mg/kg/d) for two consecutive days prior to exposing them to cold. We would then be able to assess autophagic flux by immunoblotting LC3BII and p62 [70]. We could also use laser scanning confocal microscopy to three dimensionally reconstruct whole-mount structures of BAT and assess immunostains of LC3 and lysosomal Lamp-2 co-localization [121]. To

add, most studies investigating AMPK and autophagy examine its role in the initiation of phagophore formation through the activation of ULK1. It has recently been shown, in skeletal muscle, that transcription factor EB (TFEB), the master regulator of lysosomal biogenesis, is a potential target for PGC-1α in the regulation of autophagy, and thus, the tie between AMPK and TFEB and other mediators of the autophagic pathway should be examined [122].

In our current study, we were able to visualize altered ultra-structures within the lipid bilayer of the cristae, suggesting a defect in the formation of "cristae junctions". In 1998, Perkins and colleagues identified cristae junctions in brown adipocytes (for review see [123]) as narrow, tubular openings that attach cristae to the inner boundary membrane of the IMM that may have an impact on the distribution of proteins in the IMM [124]. The distribution of proteins between the inner boundary membrane and cristae membrane could have implications in fundamental processes of mitochondria including, but not limited to, oxidative phosphorylation, protein translocation, metabolite exchange, fission and fusion, degradation, and apoptosis [125]. Thus, perhaps cristae junctions have a role in the ability of BAT and beige mitochondria to promote energy utilization through non-shivering thermogenesis.

Last, our results suggest that adipocyte AMPK could be a promising therapeutic target for the treatment of metabolic diseases by promoting BAT activity and the browning of WAT. To test this, Control and iβ1β2AKO mice could be fed a 45 % high-fat diet for 12 weeks, with a masking agent or a novel adipose tissue-specific AMPK activator. Technologies such as the cell-SELEX can select adipocyte-specific aptamers,

for instance adipo-8, to bind with high affinity only to adipocytes [126]. These aptamers could potentially be used as a tool to deliver drugs specifically to adipose tissue, in our case AMPK activators and be tested for therapeutic treatment of metabolic disease. Of course, this technology needs to be developed further, and may not be implemented due to the high cost of production, but could help further establish the importance of AMPK activation in adipose to promote non-shivering thermogenesis and subsequent metabolic benefits.

CHAPTER VI – CONCLUSION

CHAPTER VI – CONCLUSION

This thesis examines the *in vivo* role of AMPK in the metabolic function of brown and beige adipose tissue. We generated a novel, inducible, and adipose tissue-specific AMPK knockout mouse model and found that iβ1β2AKO mice are intolerant to cold, resistant to inducing UCP1-mediated thermogenesis in response to β3-AR activation, are unable to adapt to chronic β3-AR activation in both BAT and WAT, and have reduced BAT mitochondrial integrity due to a defect in autophagy/mitophagy. These findings provide strong evidence that adipocyte AMPK in BAT regulates a fine-tuned program that responds to environmental (cold) and pharmacological (CL-316,243) inputs to maintain mitochondrial integrity through autophagy, and increases mitochondrial biogenesis in response to chronic β-adrenergic stimuli. To add, AMPK effects seem dependent on the adipose tissue being examined. Further investigation is required to determine differential mechanisms mediating these effects.

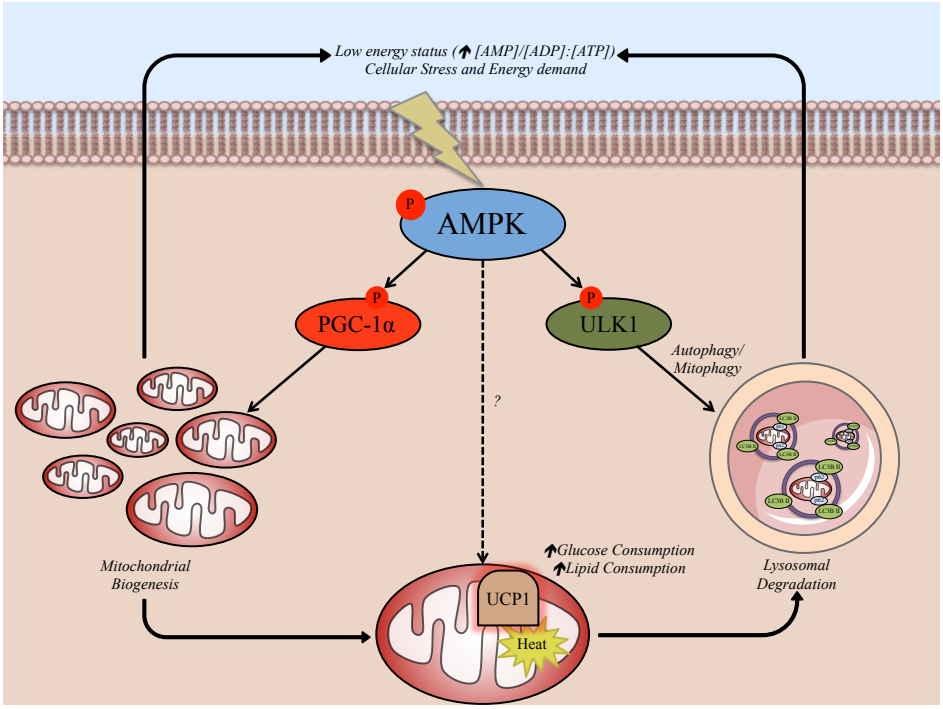

REFERENCES

REFERENCES

1. Ng, M. *et al.* Global , regional and national prevalence of overweight and obesity in children and adults 1980-2013 : A systematic analysis. *Lancet* **384,** 766–781 (2014).
2. World Health Organization. Obesity. **N 311,** (2014).
3. American Association of Clinical Endocrinologists *et al. Resolution: Recognition of Obesity as a Disease*. **420,** (A–13) (2013).
4. The NCD Risk Factor Collaboration Team. The weight of the world – trends in adult body mass index in 200 countries since 1975: pooled analysis of 1,698 population-based measurement studies with 19.2 million participants. *Lancet* (2016).
5. World Health Organization. *Ending Childhood Obesity*. (2016).
6. Statistics Canada. *Mortality , Summary List of Causes*. (2009).
7. Wang, Y., Beydoun, M. A., Liang, L., Caballero, B. & Kumanyika, S. K. Will All Americans Become Overweight or Obese ? Estimating the Progression and Cost of the US Obesity Epidemic. *Obesity* **16,** 2323–2330 (2008).
8. Unger, R. H. Lipotoxic iseases. *Annu. Rev. Med.* **53,** 319–336 (2002).
9. Lee, Y. *et al.* B-Cell lipotoxicity in the pathogenesis of non-insulin-dependent diabetes mellitus of obese rats : Impairment in adipocyte- B-cell relationships. *Proc. Natl. Acad. Sci.* **91,** 10878–10882 (1994).
10. Zhou, Y. *et al.* Lipotoxic heart disease in obese rats : Implications for human obesity. *Proc. Natl. Acad. Sci.* **97,** 1784–1789 (2000).

11. Koyama, K. *et al.* Tissue triglycerides, insulin resistance, and insulin production: implications for hyperinsulinemia of obesity. *Am. J. Physiol. Endocrinol. Metab.* **273,** E708–E713 (1997).

12. Cook, K. S. *et al.* Adipsin: a circulating serine protease homolog secreted by adipose tissue and sciatic nerve. *Science (80-.).* **237,** 402–405 (1987).

13. Zhang, Y. *et al.* Positional cloning of the mouse obese gene and its human homologue. *Nature* **372,** 425–432 (1994).

14. Galic, S., Oakhill, J. S. & Steinberg, G. R. Molecular and Cellular Endocrinology Adipose tissue as an endocrine organ. *Mol. Cell. Endocrinol.* **316,** 129–139 (2010).

15. Kershaw, E. E. & Flier, J. S. Adipose Tissue as an Endocrine Organ. *J. Clin. Endocrinol. Metab.* **89,** 2548–2556 (2016).

16. Unger, R. H. & Scherer, P. E. Gluttony, sloth and the metabolic syndrome: a roadmap to lipotoxicity. *Trends Endocrinol. Metab.* **21,** 345–352 (2010).

17. Rosen, E. D. & Spiegelman, B. M. What We Talk About When We Talk About Fat. *Cell* **156,** 20–44 (2014).

18. Wajchenberg, B. L., Giannella-Neto, D., da Silva, M. E. R. & Santos, R. F. Depot-Specific Hormonal Characteristics of Subcutaneous and Visceral Adipose Tissue and their Relation to the Metabolic Syndrome. *Horm. Metab. Res.* **34,** 616–621 (2002).

19. Bjorntorp, P. ‘ Portal ’ Adipose Tissue as a Generator of Risk Factors for Cardiovascular Disease and Diabetes. *Arteriosclerosis* **10,** 493–497 (1990).

20. Cannon, B. & Nedergaard, J. Brown Adipose Tissue: Function and Physiological

Significance. *Physiol. Rev.* **84,** 277–359 (2004).

21. Yoneshiro, T. *et al.* Brown Adipose Tissue, Whole-Body Energy Expenditure, and Thermogenesis in Healthy Adult Men. *Obesity* **19,** 13–16 (2011).
22. van Marken Lichtenbelt, W. Brown adipose tissue and the regulation of nonshivering thermogenesis. *Curr. Opin. Clin. Nutr. Metab. Care* **15,** 547–552 (2012).
23. Young, P., Arch, J. R. S. & Ashwell, M. Brown adipose tissue in the parametrial fat pad of the mouse. *FEBS Lett.* **167,** 10–14 (1984).
24. Wu, J. *et al.* Beige Adipocytes Are a Distinct Type of Thermogenic Fat Cell in Mouse and Human. *Cell* **150,** 366–376 (2012).
25. Hany, T. F. *et al.* Brown adipose tissue : a factor to consider in symmetrical tracer uptake in the neck and upper chest region. *Eur. J. Nucl. Med.* **29,** 1393–1398 (2002).
26. Yeung, H. W. D., Grewal, R. K., Gonen, M., Schoder, H. & Larson, S. M. Patterns of 18 F-FDG Uptake in Adipose Tissue and Muscle : A Potential Source of. *J. Nucl. Med.* **44,** 1789–1797 (2003).
27. Nedergaard, J., Bengtsson, T. & Cannon, B. Unexpected evidence for active brown adipose tissue in adult humans. *Am. J. Physiol. Endocrinol. Metab.* **293,** 444–452 (2007).
28. Saito, M. *et al.* High Incidence of Metabolically Active Brown Adipose Effects of Cold Exposure and Adiposity. *Diabetes* **58,** 1526–1531 (2009).
29. Cypess, A. M. *et al.* Identification and importance of brown adipose tissue in adult

humans. *N. Engl. J. Med.* **360,** 1509–1517 (2009).

30. van Marken Lichtenbelt, W. D. *et al.* Cold-activated brown adipose tissue in healthy men. *N. Engl. J. Med.* **360,** 1500–1508 (2009).

31. Virtanen, K. A. *et al.* Functional Brown Adipose Tissue in Healthy Adults. *N. Engl. J. Med.* **360,** 1518–1525 (2009).

32. Nicholls, D. G. & Locke, R. M. Thermogenic Mechanisms in Brown Fat. *Physiol. Rev.* **64,** 1–64 (1984).

33. Heaton, G. M., Wagenvoord, R. J., Kemp JR, A. & Nicholls, D. G. Brown-Adipose-Tissue Mitochondria : Photoaffinity Labelling of the Regulatory Site of Energy Dissipation. *Eur. J. Biochem.* **82,** 515–521 (1978).

34. Kiens, B., Alsted, T. J. & Jeppesen, J. Factors regulating fat oxidation in human skeletal muscle. *Obes. Rev.* **12,** 852–858 (2011).

35. Nicholls, D. G. & Rial, E. A History of the First Uncoupling Protein , UCP1. *J. Bioenerg. Biomembr.* **31,** 399–406 (1999).

36. Fedorenko, A., Lishko, P. V & Kirichok, Y. Mechanism of Fatty-Acid-Dependent UCP1 Uncoupling in Brown Fat Mitochondria. *Cell* **151,** 400–413 (2012).

37. Nnodim, J. O. & Lever, J. D. Neural and Vascular Provisions of Rat lnterscapular Brown Adipose Tissue. *Am. J. Anat.* **182,** 283–293 (1988).

38. Smith, R. E. & Roberts, J. C. Thermogenesis of brown adipose tissue in cold-acclimated rats. *Am. J. Physiol.* **206,** 143–148 (1964).

39. Harms, M. & Seale, P. Brown and beige fat : development , function and therapeutic potential. *Nat. Med.* **19,** 1252–1263 (2013).

40. Cao, W. *et al.* p38 Mitogen-Activated Protein Kinase Is the Central Regulator of Cyclic AMP-Dependent Transcription of the Brown Fat Uncoupling Protein 1 Gene. *Mol. Cell. Biol.* **24,** 3057–3067 (2004).

41. Contreras, C. *et al.* The brain and brown fat. *Ann. Med.* **47,** 150–168 (2015).

42. Lee, P., Swarbrick, M. M. & Ho, K. K. Y. Brown Adipose Tissue in Adult Humans : A Metabolic Renaissance. *Endocr. Rev.* **34,** 413–438 (2013).

43. Hardie, D. G., Ross, F. A. & Hawley, S. A. AMPK : a nutrient and energy sensor that maintains energy homeostasis. *Nat. Rev. Mol. Cell Biol.* **13,** 251–262 (2012).

44. Steinberg, G. R. & Kemp, B. E. AMPK in Health and Disease. *Physiol. Rev.* **89,** 1025–1078 (2009).

45. Stapleton, D. *et al.* Mammlian AMP-activated Protein Kinase Subfamily*. *J. Biol. Chem.* **271,** 611–615 (1996).

46. Thornton, C., Snowden, M. A. & Carling, D. Identification of a Novel AMP-activated Protein Kinase B Subunit Isoform That Is Highly Expressed in Skeletal Muscle*. *J. Biol. Chem.* **273,** 12443–12450 (1998).

47. Cheung, P. C. F., Salt, I. P., Davies, S. P., Hardie, D. G. & Carling, D. Characterization of AMP-acitvated protein kinase y-subunit isoforms and their role in AMP binding. *Biochem. J.* **669,** 659–669 (2000).

48. Hardie, D. G. AMPK—Sensing Energy while Talking to Other Signaling Pathways. *Cell Metab.* **20,** 939–952 (2014).

49. Stein, S. C., Woods, A., Jones, N. A., Davison, M. D. & Carling, D. The regulation of AMP-activated protein kinase by phosphorylation. *Biochem. J.* **345,** 437–443

(2000).

50. Gowans, G. J., Hawley, S. A., Ross, F. A. & Hardie, D. G. AMP Is a True Physiological Regulator of AMP-Activated Protein Kinase by Both Allosteric Activation and Enhancing Net Phosphorylation. *Cell Metab.* **18,** 556–566 (2013).

51. Davies, S. P., Helps, N. R., Cohen, P. T. W. & Hardie, D. G. 5 ' -AMP inhibits dephosphorylation , as well as promoting phosphorylation , of the AMP-activated protein kinase . Studies using bacterially expressed human protein phosphatase-2Ca and native bovine protein phosphatase-2Ac. *FEBS Lett.* **377,** 421–425 (1995).

52. Hawley, S. A. *et al.* Characterization of the AMP-activated Protein Kinase Kinase from Rat Liver and Identification of Threonine 172 as the Major Site at Which It Phosphorylates AMP-activated Protein Kinase *. *J. Biol. Chem.* **271,** 27879–27887 (1996).

53. Andersson, U. *et al.* AMP-activated Protein Kinase Plays a Role in the Control of Food Intake *. *J. Biol. Chem.* **279,** 12005–12009 (2004).

54. Fullerton, M. D. *et al.* Single phosphorylation sites in Acc1 and Acc2 regulate lipid homeostasis and the insulin-sensitizing effects of metformin. *Nat. Med.* **19,** 1649–1654 (2013).

55. Lebrasseur, N. K. *et al.* Thiazolidinediones can rapidly activate AMP-activated protein kinase in mammalian tissues. *Am. J. Physiol. Endocrinol. Metab.* **291,** 175–181 (2006).

56. Hawley, S. A. *et al.* The Ancient Drug Salicylate Directly Activates AMP-Activated Protein Kinase. *Science (80-.).* **336,** 918–922 (2012).

57. Carlson, C. A. & Kim, K.-H. Regulation of hepatic acetly coenzyme A carboxylase by phosphorylation and dephosphorylation*. *J. Biol. Chem.* **248,** 378–380 (1973).

58. Munday, M. R. Regulation of mammalian acetyl-CoA carboxylase. *Biochem. Soc. Trans.* **30,** 1059–1064 (2002).

59. Puigserver, P. *et al.* A Cold-Inducible Coactivator of Nuclear Receptors Linked to Adaptive Thermogenesis. *Cell* **92,** 829–839 (1998).

60. Puigserver, P. & Spiegelman, B. M. Peroxisome Proliferator-Activated Receptor-y Coactivator 1 a (PGC-1 a): Transcriptional Coactivator and Metabolic Regulator. *Endocr. Rev.* **24,** 78–90 (2003).

61. Jager, S., Handschin, C., St-Pierre, J. & Spiegelman, B. M. AMP-activated protein kinase (AMPK) action in skeletal muscle via direct phosphorylation of PGC-1a. *Proc. Natl. Acad. Sci.* **104,** 12017–12022 (2007).

62. Iwabu, M. *et al.* Adiponectin and AdipoR1 regulate PGC-1 a and mitochondria by Ca and AMPK / SIRT1. *Nature* **464,** 1313–1319 (2010).

63. Wu, Z. *et al.* Mechanisms Controlling Mitochondrial Biogenesis and Respiration through the Thermogenic Coactivator PGC-1. *Cell* **98,** 115–124 (1999).

64. Barbera, M. J. *et al.* Peroxisome Proliferator-activated Receptor a Activates Transcription of the Brown Fat Uncoupling Protein-1 Gene: A Link Between Regulation of the Thermogenic and Lipid Oxidation Pathways in the Brown Fat Cell. *J. Biol. Chem.* **276,** 1486–1493 (2001).

65. Egan, D. F. *et al.* Phosphorylation of ULK1 (hATG1) by AMP-Activated Protein Kinase Connects Energy Sensing to Mitophagy. *Science (80-.).* **331,** 456–462

(2011).

66. Kim, I., Rodriguez-Enriquez, S. & Lemasters, J. J. Selective degradation of mitochondria by mitophagy. *Arch. Biochem. Biophys.* **462,** 245–253 (2007).

67. Twig, G. *et al.* Fission and selective fusion govern mitochondrial segregation and elimination by autophagy. *EMBO J.* **27,** 433–446 (2008).

68. Kim, J., Kundu, M., Viollet, B. & Guan, K. AMPK and mTOR regulate autophagy through direct phosphorylation of Ulk1. *Nat. Cell Biol.* **13,** 132–141 (2011).

69. Wong, P., Puente, C., Ganley, I. G. & Jiang, X. The ULK1 complex: Sensing nutrient signals for autophagy activation. *Autophagy* **9,** 124–137 (2013).

70. Klionsky, D. J. *et al.* Guidelines for the use and interpretation of assays for monitoring autophagy. *Autophagy* **8,** 445–544 (2012).

71. Füllgrabe, J., Klionsky, D. J. & Joseph, B. The return of the nucleus: transcriptional and epigenetic control of autophagy. *Nat. Rev. Mol. Cell Biol.* **15,** 65–74 (2014).

72. Bjørkøy, G. *et al.* p62/SQSTM1 forms protein aggregates degraded by autophagy and has a protective effect on huntingtin-induced cell death. *J. Cell Biol.* **171,** 603–614 (2005).

73. Tanaka, A. Parkin-mediated selective mitochondrial autophagy , mitophagy : Parkin purges damaged organelles from the vital mitochondrial network. *FEBS Lett.* **584,** 1386–1392 (2010).

74. Mulligan, J. D., Gonzalez, A. A., Stewart, A. M., Carey, H. V & Saupe, K. W. Upregulation of AMPK during cold exposure occurs via distinct mechanisms in

brown and white adipose tissue of the mouse. *J. Physiol.* **580,** 677–684 (2007).

75. Pulinilkunnil, T. *et al.* Adrenergic Regulation of AMP-activated Protein Kinase in Brown Adipose Tissue in Vivo. *J. Biol. Chem.* **286,** 8798–8809 (2011).

76. Bauwens, J. D. *et al.* Cold tolerance, cold-induced hyperphagia, and nonshivering thermogenesis are normal in α_1-AMPK-/- mice. *Am. J. Physiol. Regul. Integr. Comp. Physiol.* **301,** R473–R483 (2011).

77. Crane, J. D., Mottillo, E. P., Farncombe, T. H., Morrison, K. M. & Steinberg, G. R. A standardized infrared imaging technique that specifically detects UCP1-mediated thermogenesis invivo. *Mol. Metab.* **3,** 490–494 (2014).

78. Mottillo, E. P., Shen, X. J. & Granneman, J. G. Role of hormone-sensitive lipase in β-adrenergic remodeling of white adipose tissue. *Am. J. Physiol. Endocrinol. Metab.* **293,** 1188–1197 (2007).

79. Mottillo, E. P. *et al.* Coupling of lipolysis and de novo lipogenesis in brown, beige, and white adipose tissues during chronic β3-adrenergic receptor activation. *J. Lipid Res.* **55,** 1–33 (2014).

80. O'Neill, H. M. *et al.* AMP-activated protein kinase (AMPK) beta1beta2 muscle null mice reveal an essential role for AMPK in maintaining mitochondrial content and glucose uptake during exercise. *Proc. Natl. Acad. Sci. U. S. A.* **108,** 16092–7 (2011).

81. Folch, J., Lees, M. & Sloane Stanley, G. H. A simple method for the isolation and purification of total lipides from animal tissues. *J. Biol. Chem.* **226,** 497–509 (1957).

82. Li, X. *et al.* Electron counting and beam-induced motion correction enable near-atomic-resolution single-particle cryo-EM. *Nat. Methods* **10,** 584–590 (2013).

83. Poole, A. C. *et al.* The PINK1 / Parkin pathway regulates mitochondrial morphology. *Proc. Natl. Acad. Sci.* **105,** 1638–1643 (2008).

84. Steinberg, G. R. *et al.* Fatty acid oxidation and triacylglycerol hydrolysis are enhanced after chronic leptin treatment in rats. *Am. J. Physiol. Endocrinol. Metab.* **282,** 593–600 (2002).

85. Cannon, B. & Nedergaard, J. Studies of Thermogenesis and Mitochondrial Function in Adipose Tissues. *Methods Mol. Biol.* **456,** 109–121 (2008).

86. Shabalina, I. *et al.* UCP1 in Brite/Beige adipose tissue mitochondria is functionally thermogenic. *Cell Rep.* **5,** 1196–1203 (2013).

87. Iseli, T. J. *et al.* AMP-activated Protein Kinase B Subunit Tethers a and y Subunits via Its C-terminal Sequence (186 – 270)*. *J. Biol. Chem.* **280,** 13395–13400 (2005).

88. Ya, R. & Downs, S. M. Suppression of Chemically Induced and Spontaneous Mouse Oocyte Activation by AMP-Activated Protein Kinase. *Biol. Reprod.* **88,** Article 70, 1–11 (2013).

89. Zhang, H. *et al.* MicroRNA- 455 regulates brown adipogenesis via a novel HIF 1 an-AMPK-PGC 1 a signaling network. *EMBO Rep.* **16,** 1378–1393 (2015).

90. Silva, K. R. *et al.* Stromal-vascular fraction content and adipose stem cell behavior are altered in morbid obese and post bariatric surgery ex-obese women. *Stem Cell Res. Ther.* **6,** 1–13 (2015).

91. O'Neill, H. M., Holloway, G. P. & Steinberg, G. R. AMPK regulation of fatty acid metabolism and mitochondrial biogenesis: Implications for obesity. *Mol. Cell. Endocrinol.* **366,** 135–151 (2013).

92. Samari, H. R. & Seglen, P. O. Inhibition of Hepatocytic Autophagy by Adenosine , Aminoimidazole- 4-carboxamide Riboside , and N 6 -Mercaptopurine Riboside: Evidense for Involvement of AMP-Activated Protein Kinase*. *J. Biol. Chem.* **273,** 23758–23763 (1998).

93. Bujak, A. L. *et al.* AMPK Activation of Muscle Autophagy Prevents Fasting-Induced Hypoglycemia and Myopathy during Aging. *Cell Metab.* **21,** 883–890 (2015).

94. Rosenbaum, M. & Leibel, R. L. Adaptive thermogenesis in humans. *Int. J. Obes.* **34,** S47–S55 (2010).

95. Fothergill, E. *et al.* Persistent Metabolic Adaptation 6 Years After ' The Biggest Loser ' Competition. *Obesity* **00,** 1–8 (2016).

96. Hutchinson, D. S., Chernogubova, E., Dallner, O. S., Cannon, B. & Bengtsson, T. Beta-adrenoceptors, but not alpha-adrenoceptors, stimulate AMP-activated protein kinase in brown adipocytes independently of uncoupling protein-1. *Diabetologia* **48,** 2386–95 (2005).

97. Inokuma, K. *et al.* Uncoupling Protein 1 Is Necessary for Norepinephrine-Induced Glucose Utilization in Brown Adipose Tissue. *Diabetes* **54,** 1385–1391 (2005).

98. Gauthier, M.-S. *et al.* AMP-activated Protein Kinase Is Activated as a Consequence of Lipolysis in the Adipocyte POTENTIAL MECHANISM AND

PHYSIOLOGICAL RELEVANCE *. *J. Biol. Chem.* **283,** 16514–16524 (2008).

99. Koh, H. *et al.* Adrenaline is a critical mediator of acute exercise-induced AMP-activated protein kinase activation in adipocytes. *Biochem. J.* **481,** 473–481 (2007).

100. Watt, M. J., Steinberg, G. R., Chen, Z., Kemp, B. E. & Febbraio, M. A. Fatty acids stimulate AMP-activated protein kinase and enhance fatty acid oxidation in L6 myotubes. *J. Physiol.* **1,** 139–147 (2006).

101. Lee, J., Ellis, J. M. M. & Wolfgang, M. J. J. Adipose Fatty Acid Oxidation Is Required for Thermogenesis and Potentiates Oxidative Stress-Induced Inflammation. *Cell Rep.* **10,** 266–279 (2015).

102. Ducommun, S. *et al.* Motif affinity and mass spectrometry proteomic approach for the discovery of cellular AMPK targets : Identification of mitochondrial fi ssion factor as a new AMPK substrate. *Cell. Signal.* **27,** 978–988 (2015).

103. Zhang, C. & Lin, S. AMPK Promotes Autophagy by Facilitating Mitochondrial Fission. *Cell Metab.* **23,** 399–401 (2016).

104. Müller, T. D. *et al.* p62 Links β -adrenergic input to mitochondrial function and thermogenesis. *J. Clin. Invesitgation* **123,** 469–478 (2013).

105. Ro, S.-H. *et al.* Distinct functions of Ulk1 and Ulk2 in the regulation of lipid metabolism in adipocytes Distinct functions of Ulk1 and Ulk2 in the regulation of lipid metabolism in adipocytes. *Autophagy* **9,** 2103–2114 (2013).

106. Chondronikola, M. *et al.* Brown Adipose Tissue Improves Whole-Body Glucose Homeostasis and Insulin Sensitivity in Humans. *Diabetes* **63,** 4089–4099 (2014).

107. Hanssen, M. J. W. *et al.* Short-term cold acclimation improves insulin sensitivity in

patients with type 2 diabetes mellitus. *Nat. Med.* **21,** 863–865 (2015).

108. Cypess, A. M. *et al.* Activation of Human Brown Adipose Tissue by a β3-Adrenergic Receptor Agonist. *Cell Metab.* **21,** 33–38 (2015).

109. Ruderman, N. B., Carling, D., Prentki, M. & Cacicedo, J. M. AMPK , insulin resistance , and the metabolic syndrome. *J. Clin. Invesitgation* **123,** 2764–2772 (2013).

110. Yavari, A. *et al.* Chronic Activation of y 2 AMPK Induces Obesity and Reduces B Cell Function. 821–836 (2016). doi:10.1016/j.cmet.2016.04.003

111. López, M. *et al.* Hypothalamic AMPK and fatty acid metabolism mediate thyroid regulation of energy balance. *Nat. Med.* **16,** 997–1004 (2010).

112. Zhou, G. *et al.* Role of AMP-activated protein kinase in mechanism of metformin action. *J. Clin. Invesitgation* **108,** 1167–1174 (2001).

113. Quevedo, S., Roca, P., Pico, C. & Palou, A. Sex-associated differences in cold-induced UCP1 synthesis in rodent brown adipose tissue. *Pflugers Arch* **436,** 689–695 (1998).

114. Justo, R. *et al.* Gender-related differences in morphology and thermogenic capacity of brown adipose tissue mitochondrial subpopulations. *Life Sci* **76,** 1147–1158 (2005).

115. Maddineni, S., Metzger, S., Oco, O., Iii, G. H. & Ramachandran, R. Adiponectin Gene Is Expressed in Multiple Tissues in the Chicken : Food Deprivation Influences Adiponectin Messenger Ribonucleic Acid Expression. *Endocrinology* **146,** 4250–4256 (2005).

116. Morentin, M. De *et al.* Estradiol Regulates Brown Adipose Tissue Thermogenesis via Hypothalamic AMPK. *Cell Metab.* **20,** 41–53 (2014).

117. Jeffery, E. *et al.* Characterization of Cre recombinase models for the study of adipose tissue. *Adipocyte* **3,** 206–211 (2014).

118. Berry, R. & Rodeheffer, M. S. Characterization of the adipocyte cellular lineage in vivo. *Nat. Cell Biol.* **15,** 302–308 (2013).

119. Lee, K. Y. *et al.* Lessons on Conditional Gene Targeting in Mouse. *Diabetes* **62,** 864–874 (2013).

120. Lodhi, I. J. *et al.* Inhibiting Adipose Tissue Lipogenesis Reprograms Thermogenesis and PPAR g Activation to Decrease Diet-Induced Obesity. *Cell Metab.* **16,** 189–201 (2012).

121. Martinez-Santibanez, G., Cho, K. W. & Lumeng, C. N. Imaging white adipose tissue with confocal microscopy. *Methods Enzymol.* **537,** 17–30 (2014).

122. Vainshtein, A., Desjardins, E. M., Armani, A., Sandri, M. & Hood, D. A. PGC-1 α modulates denervation-induced mitophagy in skeletal muscle. *Skelet. Muscle* **5,** 1–17 (2015).

123. Zick, M., Rabl, R. & Reichert, A. S. Cristae formation — linking ultrastructure and function of mitochondria. *BBA - Mol. Cell Res.* **1793,** 5–19 (2009).

124. Perkins, G. A. *et al.* Electron Tomography of Mitochondria from Brown Adipocytes Reveals Crista Junctions. *J. Bioenerg. Biomembr.* **30,** 431–442 (1998).

125. Vogel, F., Neupert, W. & Reichert, A. S. Dynamic subcompartmentalization of the mitochondrial inner membrane. *J. Cell Biol.* **175,** 237–247 (2006).

126. Liu, J. *et al.* Selection of Aptamers Specific for Adipose Tissue. *PLoS One* **7,** e37789 (2012).

APPENDIX

APPENDIX

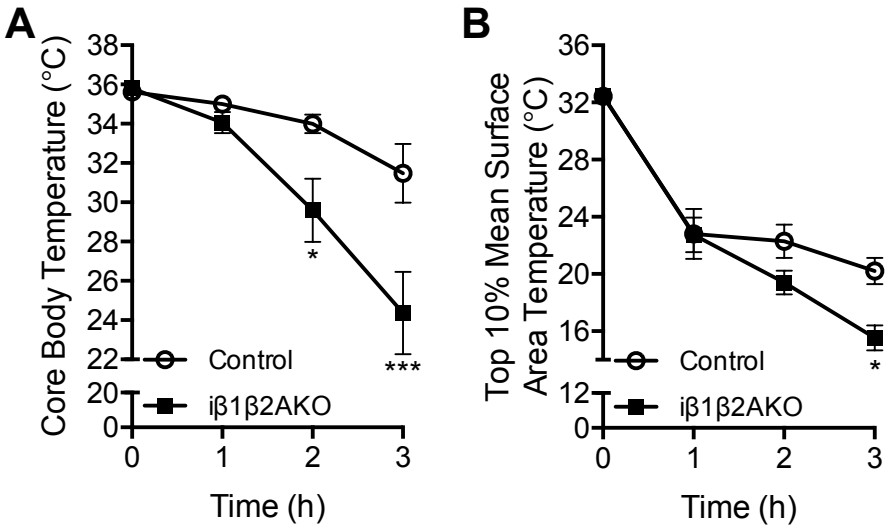

Figure 1. Core body temperature (A), and interscapular BAT surface area temperature (B) of male Control and iβ1βAKO mice at room temperature (23 °C) and cold exposed (4 °C) for 1-3 hours (n = 3-4 per group). * $p<0.05$ and *** $p<0.001$ indicates a genotype difference determined via 2-way ANOVA and Bonferroni *post hoc*.

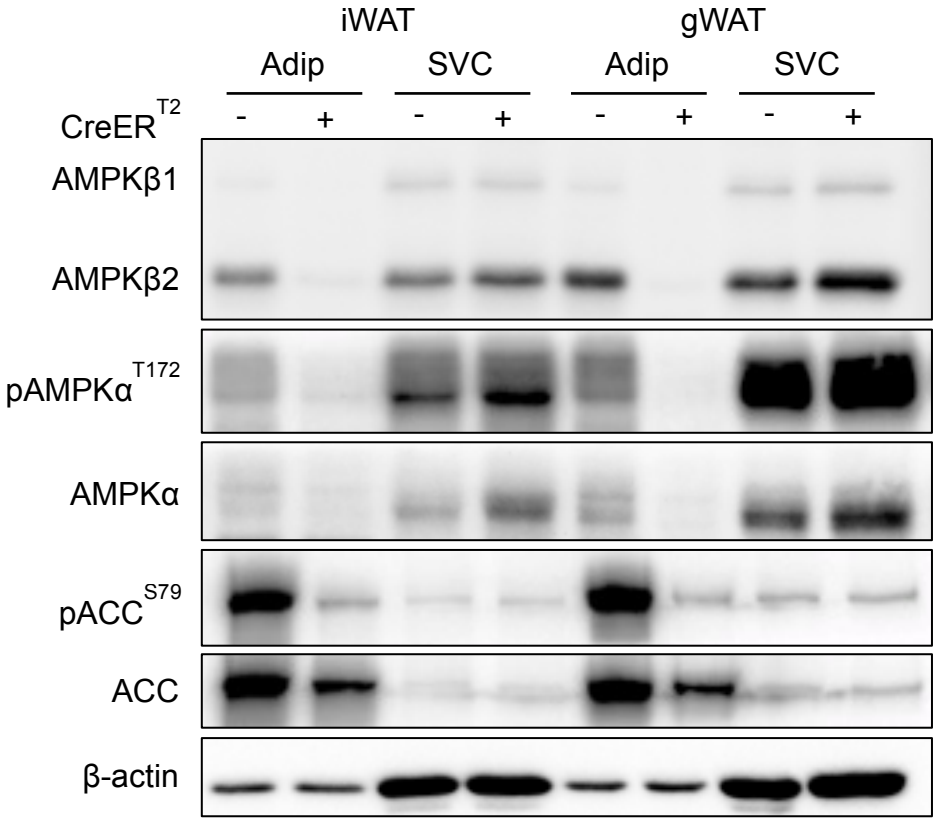

Figure 2. Representative immunoblotting of isolated adipocytes and stromal vascular cell fractions in inguinal (iWAT) and gonadal (gWAT) white adipose tissue of Control (CreER^{T2} –) and iβ1βAKO (CreER^{T2} +) mice.